10

Liquid Flows in Microchannels

Kendra V. Sharp
Pennsylvania State University

Ronald J. Adrian
University of Illinois at Urbana–Champaign

Juan G. Santiago
Stanford University

Joshua I. Molho
Caliper Life Sciences Incorporated

10.1   Introduction

Nominally, microchannels can be defined as channels whose dimensions are less than 1 millimeter and greater than 1 micron. Above 1 millimeter the flow exhibits behavior that is the same as most macroscopic flows. Currently, microchannels have characteristic dimensions anywhere from the submicron scale to hundreds of microns. Microchannels can be fabricated in many materials — glass, polymers, silicon, metals — using various processes including surface micromachining, bulk micromachining, molding, embossing, and conventional machining with microcutters. These methods and the characteristics of the resulting flow channels are discussed elsewhere in this handbook.

Microchannels offer advantages due to their high surface-to-volume ratio and their small volumes. The large surface-to-volume ratio leads to high rate of heat and mass transfer, making microdevices excellent tools for compact heat exchangers. For example, the device in Figure 10.1 is a cross-flow heat exchanger constructed from a stack of 50 14 mm $\times$ 14 mm foils, each containing 34 200 μm wide by 100 μm deep
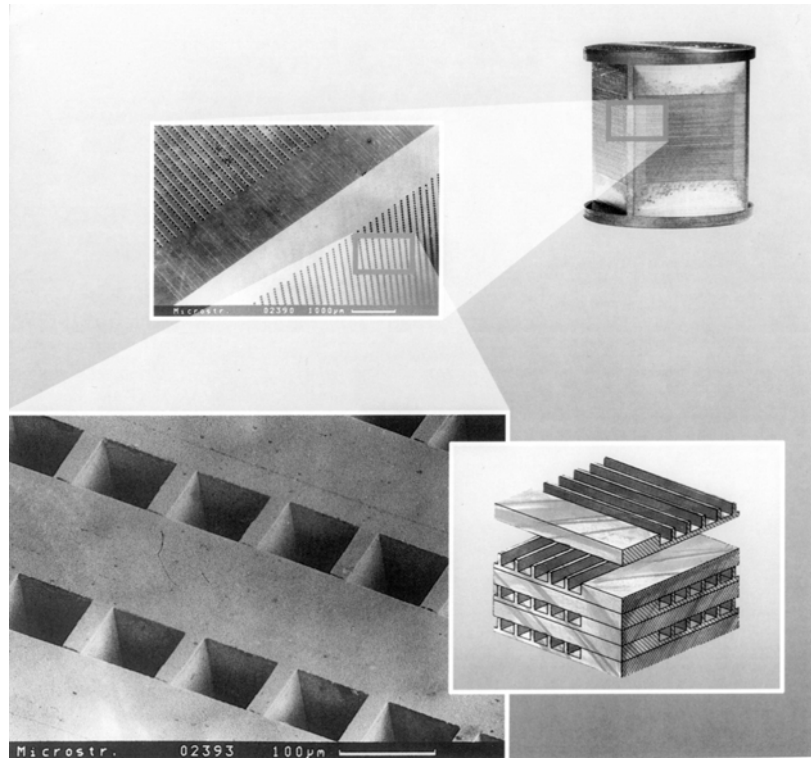
FIGURE 10.1   Micro heat exchanger constructed from rectangular channels machined in metal. (Reprinted with permission from K. Schubert and D. Cacuci, Forschungszentrum, Karlsruhe.)

AQ35

channels machined into the 200 μm thick stainless steel foils by the process of direct, high-precision mechanical micromachining [Brandner et al., 2000; Schaller et al., 1999]. The direction of flow in adjacent foils is alternated 90°, and the foils are attached by means of diffusion bonding to create a stack of cross-flow heat exchangers capable of transferring 10 kW at a temperature difference of 80 K using water flowing at 750 kg/hr. The impressively high rate of heat transfer is accomplished mainly by the large surface area covered by the interior of the microchannel: approximately 3,600 mm^2 packed into a 14 mm cube.

A second example of the application of microchannels is in the area of MEMS devices for biological and chemical analysis. The primary advantage of microscale devices in these applications are the good match with the scale of biological structures and the potential for placing multiple functions for chemical analysis on a small area; that is, the concept of a chemistry laboratory on a chip.

Microchannels are used to transport biological materials such as (in order of size) proteins, DNA, cells, and embryos or to transport chemical samples and analytes. Typical of such devices is the i-STAT blood sample analysis cartridge shown in Figure 10.2. The sample is taken onboard the chip through a port and moved through the microchannels by pressure to various sites where it is mixed with analyte and moved to a different site where the output is read. Flows in biological devices and chemical analysis microdevices are usually much slower than those in heat transfer and chemical reactor microdevices.

10.1.1   Unique Aspects of Liquids in Microchannels

Flows in microscale devices differ from their macroscopic counterparts for two reasons: the small scale makes molecular effects such as wall slip more important, and it amplifies the magnitudes of certain ordinary continuum effects to extreme levels. Consider, for example, strain rate and shear rate, which scale in proportion to the velocity scale U_s and inverse proportion to the length scale L_s. Thus, 100 mm/sec flow in a 10 μm channel experiences a shear rate of the order of $10^4 \, \text{sec}^{-1}$. Acceleration scales as U_s^2/L_s and is

FIGURE 10.2   Blood sample cartridge using microfluidic channels. (Reprinted with permission from i-Stat, East   AQ36
Windsor, New Jersey, 2000)

similarly enhanced. The effect is even more dramatic if one tries to maintain the same volume flux while scaling down. The flux scales as $Q \sim U_s L_s^2$, so at constant flux $U_s \sim L_s^{-2}$ and both shear and acceleration go as L_s^{-3}. Fluids that are Newtonian at ordinary rates of shear and extension can become non-Newtonian at very high rates. The pressure gradient becomes especially large in small cross section channels. For fixed volume flux, the pressure gradient increases as L_s^{-4}.

Electrokinetic effects occur at the interface between liquids and solids such as glass due to chemical interaction. The result is an electrically charged double layer that induces a charge distribution in a very thin layer of fluid close to the wall. Application of an electric field to this layer creates a body force capable of moving the fluid as if it were slipping over the wall. The electroosmotic effect and the electrophoretic effect (charges around particles) will be discussed in detail in a later section. Neither occurs in gases.

The effects of molecular structure are quite different in gases and liquids. If the Knudsen number (defined as $Kn = \lambda/L_s$, where λ is the mean free path in a gas and L_s is the characteristic channel dimension) is greater than 10^{-3} [Janson et al., 1999, Gad-el-Hak, 1999], nonequilibrium effects may start to occur. Modified slip boundary conditions can be used in continuum models for Knudsen numbers between 10^{-1} and 10^{-3} [Gad-el-Hak, 1999]. As the Knudsen number continues to increase, continuum assumptions and fluid theory are no longer applicable. Analysis of such flow requires consideration of different physical phenomena (see the chapter on Analytical and Computational Models for Microscale Flows in this book, Gad-el-Hak, 1999, Janson et al., 1999, Arkilic et al. 1997, and Harley et al., 1995).

Because the density of liquids is about 1000 times the density of gases, the spacing between molecules in liquids is approximately 10 times less than the spacing in gases. Liquid molecules do not have a mean free path, but following Bridgman (1923), the lattice spacing δ may be used as a similar measure. The lattice spacing δ is defined as [Probstein, 1994]

$$\delta \sim \left(\frac{\overline{V}_1}{N_A}\right)^{1/3}, \tag{10.1}$$

where $\overline{V}_1$ is the molar volume and N_A is Avogadro's number. For water, this spacing is 0.3 nm. In a $1\,\mu m$ gap and a $50\,\mu m$ diameter channel, the equivalent Knudsen numbers are 3×10^{-4} and 6×10^{-6} respectively, well within the range of obeying continuum flow. In gases, effects such as slip at the wall occur when the mean free path length of the molecules is more than about one-tenth the flow dimension (i.e., flow dimensions of order less than 650 nm in air at STP). (Note that the mean free path length of a gas is longer than the mean spacing between its molecules; see the chapter by Gad-el-Hak in this book for a detailed discussion.) In liquids this condition will not occur unless the channels are smaller than approximately 3 nm, and continuum hydrodynamics may provide a useful description at scales even smaller than this because the forces of interaction between molecules in liquids are long range. For example, Stokes' classical result for drag on a sphere is routinely applied to particles whose diameters are well below 100 nm. Thus, liquid flow in micro devices should be described adequately by continuum hydrodynamics well below dimensions of one micron.

Molecular effects in liquids are difficult to predict because the transport theory is less well developed than the kinetic theory of gases. For this reason, studies of liquid microflows in which molecular effects may play a role are much more convincing if done experimentally.

Liquids are generally considered incompressible. Consequently, the density of a liquid in microchannel flow remains very nearly constant as a function of distance along the channel, despite the very large pressure gradients that characterize microscale flow. This behavior greatly simplifies the analysis of liquid flows relative to gas flows, wherein the large pressure drop in a channel leads to large expansion and large heat capacity.

The large heat capacity of liquids relative to gases implies that the effects of internal heating due to viscous dissipation are much less significant in liquid flows. The pressure drop in microchannel flow can be very large, and since all of the work of the pressure difference against the mean flow ultimately goes into viscous dissipation, effects due to internal heating by viscous dissipation may be significant. However they will be substantially lower in liquids than in gases, and they can often be ignored allowing one to treat the liquid as a constant density, constant property fluid.

The dynamic viscosity μ of a liquid is larger than that of a gas by a factor of about 100 (c.f., Table 10.1). This implies much higher resistance to flow through the channels. The kinematic viscosity of a liquid is typically much less than the kinematic viscosity of a gas, owing to the much higher density of liquids (c.f. Table 10.1) qualitatively to the thermal conductivity and the thermal diffusivity.

Liquids in contact with solids or gases have surface tension in the interface. At the microscale, the surface tension force becomes one of the most important forces, far exceeding body forces such as gravity and electrostatic fields.

TABLE 10.1 Dynamic and Kinematic Viscosities of Typical Liquids Compared to Air at 1 Atmosphere

Fluid	Dynamic Viscosity μ [gm/cm-s]	Kinematic Viscosity ν [cm²/s]	Thermal Conductivity k [J/K s cm]	Thermal Diffusivity κ [cm²/s]
Water @15°C	0.0114	0.0114	0.0059	0.00140
Ethyl Alcohol @ 15°C	0.0134	0.0170	0.00183	0.00099
Glycerin @15°C	23.3	18.50	0.0029	0.00098
Air @15°C	0.000178	0.145	0.000253	0.202

Bubbles can occur in liquids for good or ill. Unwanted bubbles can block channels or substantially alter the flow. But bubbles can also be used to apply pressure and to perform pumping by heating and cooling the gases inside the bubble.

Particulates and droplets suspended in liquids have densities that match those of liquids more closely. Settling is much less rapid in liquids, and suspensions have the ability to follow the accelerations of the flow. This effect can also keep suspended impurities in suspension for much longer, thereby increasing the probability that an impurity will introduce unwanted behavior.

Liquids can interact with solids to form an electric double layer at the interface. This is the basis for the phenomena of electroosmosis and electrophoresis, both of which can be used to move fluid and particles in channels. These topics will be discussed in detail in a later section. Liquids can be non-Newtonian especially at the high shear rates encountered in microchannels.

10.1.2   Continuum Hydrodynamics of Pressure Driven Flow in Channels

The general continuum description of the flow of an incompressible, Newtonian fluid flow with variable properties and no body forces other than gravity (i.e., no electrical forces) consists of the incompressible continuity equation

$$\frac{\partial u_j}{\partial x_j} = 0, \tag{10.2}$$

and the momentum equation

$$\rho\left(\frac{\partial u_i}{\partial t} + u_j\frac{\partial u_i}{\partial x_j}\right) = \frac{\partial \tau_{ij}}{\partial x_j} + \rho b_i, \tag{10.3}$$

where the fluid stress is given by Stokes' law of viscosity

$$\tau_{ij} = -p\delta_{ij} + \mu\left(\frac{\partial u_i}{\partial x_j} + \frac{\partial u_j}{\partial x_i}\right). \tag{10.4}$$

Here u_i is the ith component of the velocity vector $\mathbf{u}(\mathbf{x}, t)$; ρ is the mass density [kg/m^3]; b_i is the body force per unit mass m/s^2 (often $b_i = g_i$, the gravitational acceleration), and τ_{ij} is the stress tensor N/m^2. The corresponding enthalpy equation is

$$\rho c_p\left(\frac{\partial T}{\partial t} + u_j\frac{\partial T}{\partial x_j}\right) = -\frac{\partial q_j}{\partial x_j} + \Phi, \tag{10.5}$$

where T is the temperature, and q is the heat flux J/s m^2 given by Fourier's law of heat conduction by molecular diffusion k,

$$q_i = -k\frac{\partial T}{\partial x_i}. \tag{10.6}$$

The rate of conversion of mechanical energy into heat due to internal viscous heating, is

$$\Phi = \mu\left(\frac{\partial u_i}{\partial x_j} + \frac{\partial u_j}{\partial x_i}\right)\frac{\partial u_i}{\partial x_j}. \tag{10.7}$$

Consider a long parallel duct or channel with the x-direction along the axis of the channel and the coordinates y and z in the plane perpendicular to the axis of the channel (Figure 10.3). The entering flow undergoes a transient response in which the velocity and temperature profiles change in the streamwise direction. This process continues until the flow properties become independent of the streamwise position. In this state of *fully developed velocity profile*, the velocity field is unidirectional, $u(x) = [u(y, z), 0, 0]$, and there is no acceleration of the fluid. Thus, for fully developed flow with gravitational body force g the equations become very simply

$$\rho\frac{\partial u}{\partial t} = -\frac{dp}{dx} + \rho g_x + \frac{\partial}{\partial y}\left(\mu\frac{\partial u}{\partial y}\right) + \frac{\partial}{\partial z}\left(\mu\frac{\partial u}{\partial z}\right) \tag{10.8}$$
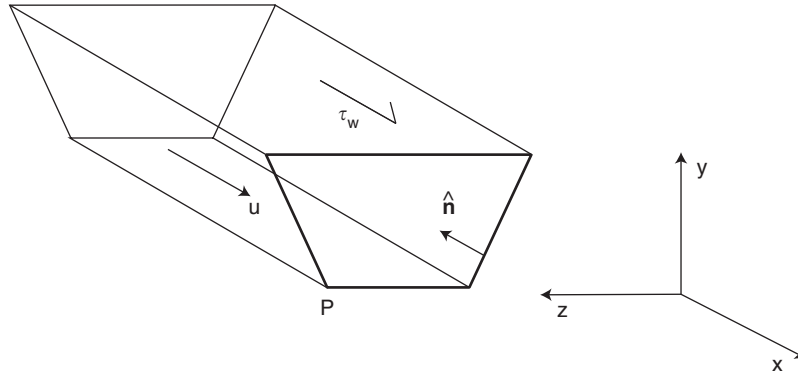
AQ4

FIGURE 10.3 Flow in a duct of arbitrary cross-section A. P is the perimeter and τ_w is the wall shear stress.

$$\rho c_p \frac{\partial T}{\partial t} = \frac{\partial}{\partial y}\left(k\frac{\partial T}{\partial y}\right) + \frac{\partial}{\partial z}\left(k\frac{\partial T}{\partial z}\right) + \Phi. \tag{10.9}$$

Lastly, if the flow is steady and the temperature and properties are constant, then the equation for streamwise velocity profiles becomes a simple Poisson equation

$$\frac{\partial^2 u}{\partial y^2} + \frac{\partial^2 u}{\partial z^2} = \frac{1}{\mu}\frac{d}{dx}(p - \rho g_x x). \tag{10.10}$$

In the absence of electrokinetic effects and for shear rates less than about $10^{12}\,\text{s}^{-1}$ the appropriate boundary condition is the no-slip condition

$$u = 0 \quad \text{on the boundary } P. \tag{10.11}$$

10.1.3 Hydraulic Diameter

Control volume analysis of fully developed flow leads naturally to the concept of the *hydraulic diameter*. Figure 10.3 shows flow in a duct of arbitrary cross-section. Since the flow is fully developed and unidirectional (assuming a straight duct), the acceleration is zero and control volume analysis of the momentum reduces to a simple force balance in the streamwise direction,

$$-\frac{dp}{dx}A = \overline{\tau}_w P \tag{10.12}$$

wherein

$$\overline{\tau}_w = \frac{1}{P}\oint_P \tau_w\, dl \tag{10.13}$$

is the wall shear stress averaged around the perimeter, and the local wall shear stress is given by

$$\tau_w = \mu\frac{\partial u}{\partial n}\bigg|_{n=0}. \tag{10.14}$$

Equation (10.12) displays the relevance of the ratio of the area A to the perimeter P. In practice, the hydraulic diameter is defined to be

$$D_h = \frac{4A}{P} \tag{10.15}$$

so that, when the cross-section is a circle, D_h equals its diameter. The hydraulic diameter provides a convenient way to characterize a duct with a single length scale and a basis for comparison between ducts of

different shapes. A common approximation is to also estimate the flow resistance in a duct or channel as the resistance of a round duct whose diameter is equal to the hydraulic diameter. This approximation is useful but subject to errors of order 10–20%. Since solution of Poisson's equation to obtain the exact wall shear stress is accomplished readily by numerical means, the approximation is not necessary.

AQ5

10.1.4 Flow in Round Capillaries

Flow in a round tube is the archetype for all duct and channel flows. While microfabrication characteristically yields channels of noncircular cross-section, the round cross-section is a useful and familiar point of reference, and microcapillaries are not uncommon. Extensive macroscale research on pipe flows dates back to Hagen's (1839), Poiseuille's (1841), and Reynolds' (1883) original studies in the 19th century. Independently, both Hagen (1839) and Poiseuille (1841) observed the relation between pressure head and velocity and its inverse proportionality to the fourth power of tube diameter.

In a round capillary of radius $a = D/2$ and radial coordinate r, it is well known that the velocity profile across a diameter is parabolic

$$u = u_{max}\left(1 - \frac{r^2}{a^2}\right) \tag{10.16}$$

where the maximum velocity is given by

$$u_{max} = \frac{a^2}{4\mu}\left(-\frac{dp}{dx}\right). \tag{10.17}$$

The volume flow rate Q is given by:

$$Q = \overline{U}A \tag{10.18}$$

where the average velocity $\overline{U}$ defined by

$$\overline{U} = \frac{1}{\pi a^2}\int_0^a u(r)2\pi r \, dr \tag{10.19}$$

is numerically equal to

$$\overline{U} = \frac{1}{2}u_{max}. \tag{10.20}$$

Using these relations it is easily shown that the pressure drop in a length L, $\Delta p = (-dp/dx)L$, is given by

$$\Delta p = \frac{8\mu LQ}{\pi a^4}. \tag{10.21}$$

The Darcy friction factor f is defined so that

$$\Delta p = f\frac{L}{D}\rho\frac{\overline{U}^2}{2} \tag{10.22}$$

(The Fanning friction factor is one-fourth of the Darcy friction factor). The Reynolds number is defined in terms of a characteristic length scale[1] L_s by

$$\text{Re} = \frac{\rho\overline{U}L_s}{\mu}. \tag{10.23}$$

For a round pipe, the characteristic length scale is the diameter of the pipe D. The friction factor for laminar flow in a round capillary is given by

$$f = \frac{64}{\text{Re}}. \tag{10.24}$$

---

[1] In the remainder of this chapter, the characteristic length scale used in calculating Re is to be inferred from context, e.g., generally D_h for a rectangular channel and D for a circular tube.

The Poiseuille number is sometimes used to describe flow resistance in ducts of arbitrary cross-section. It is defined by

$$P_O = f\,\text{Re}/4$$
$$= -\frac{1}{\mu}\frac{dp}{dx}\frac{D_h^2}{2\overline{U}}, \tag{10.25}$$

where L_s used in the calculation of Re is D_h. The Poiseuille number has a value of 16 for a round capillary.

The inverse relationship between friction factor and Reynolds number has been well documented on the macroscale. It means that the pressure drop is linearly proportional to the flow rate, Q. In the laminar region there is no dependence on surface roughness.

The pressure drops due to pressure-driven flow in microchannels are quite large. For example, water (nominally, $\mu = 10^{-3}$ kg/m-s) flowing at $Q = 0.01$ cc/sec in a $D = 100$ micron diameter, $L = 10$ mm long tube creates a pressure drop of $\Delta p = 40.7$ kN/m^2. Under these conditions the mean velocity is 1.27 msec^{-1}, and the Reynolds number is Re $= 127$. If the tube diameter is reduced to 10 microns keeping all other factors constant, the mean velocity is 127 msec^{-1}, the Reynolds number is Re $= 1270$, and the pressure drop increases to 407 MN/m^2, or 4070 atmospheres.

As the Reynolds number increases above 2000 in a circular duct, the flow begins to transition to turbulence. At this point, the friction factor increases dramatically, and the flow resistance ultimately becomes proportional to Q^2 rather than Q.

10.1.5   Entrance Length Development

Before the flow reaches the state of a fully developed velocity profile, it must transition from the profile of the velocity at the entrance to the microduct, whatever that is, to the fully developed limit. This transition occurs in the *entrance length* (L_e) of the duct. In this region the flow looks like a boundary layer that grows as it progresses downstream. Ultimately, the viscously retarded layers meet in the center of the duct at the end of the entrance length.

The pressure drop from the beginning of the duct to a location x is given by

$$p_0 - p(x) = \left(f\frac{x}{D_h} + K(x)\right)\frac{\rho\overline{U}^2}{2} \tag{10.26}$$

wherein $K(x)$ is the pressure-drop parameter given in Figure 10.4 for a circular duct and for parallel plates [White, 1991]. The flow development is largely completed by $x/D = 0.065$ Re.

10.1.6   Transition to Turbulent Flow

In 1883, Reynolds found a critical value of velocity, u_{crit}, above which the form of the flow resistance changes. The corresponding dimensionless parameter is the critical Reynolds number, Re_{crit}, below which disturbances in the flow are not maintained. Such disturbances may be caused by inlet conditions like a sharp edge or unsteadiness in the flow source. Depending on the Reynolds number, disturbances may also be introduced by natural transition to turbulent flow.

Reynolds found Re_{crit} to be approximately 2000, and this value has been generally accepted. Once the flow is fully turbulent, the empirical relationship often used to correlate friction factor and Reynolds number for smooth pipes and initially proposed by Blasius is

$$f \approx 0.3164\ \text{Re}^{-0.25}. \tag{10.27}$$

For rough pipes, the friction factor departs from the Blasius relation in the turbulent region. This departure occurs at different values of Re depending on the magnitude of the surface roughness. The Moody chart summarizes the traditional friction factor curves and is readily available in any basic fluids textbook [e.g., White, p. 318, 1994].
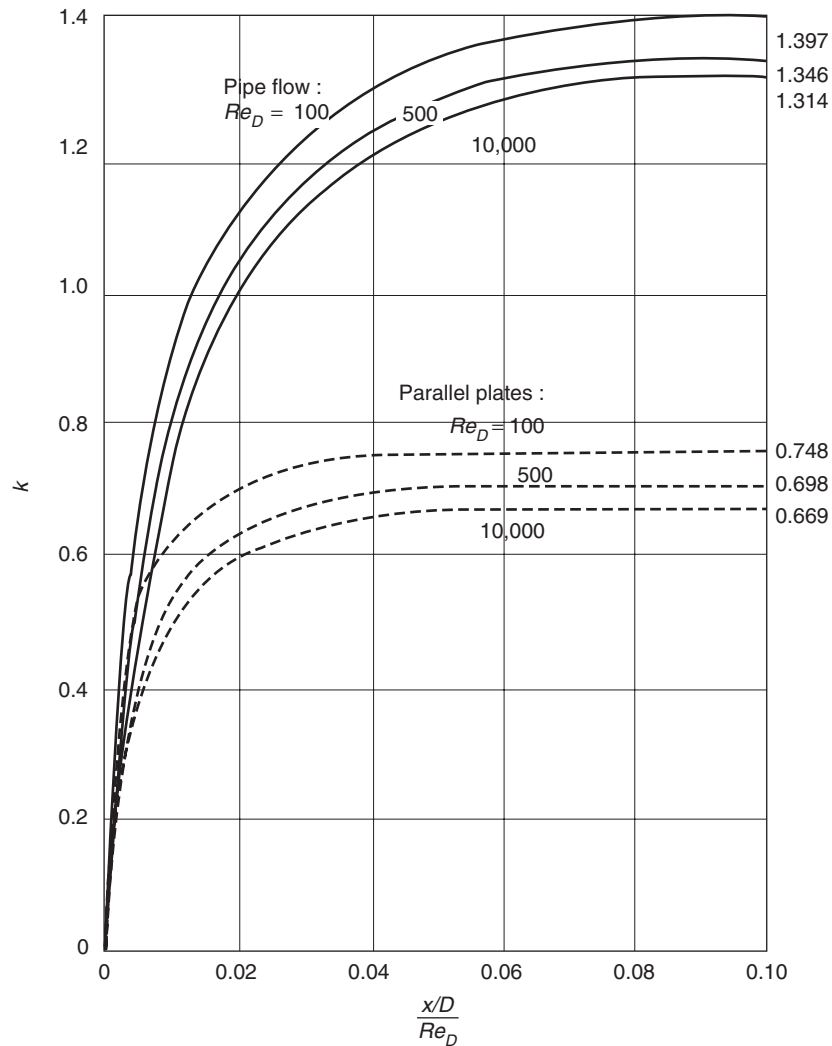
FIGURE 10.4   Entrance length parameter K for laminar flow in the inlet of a duct. (Reprinted with permission from White, F.M. [1991] *Viscous Flow*, 2nd ed., p. 292, McGraw-Hill, New York.).

10.1.7   Noncircular Channels

Microfluidic channels are generally formed by micromachining open channels on a planar substrate and closing the channels by covering the substrate with a thin plate, such as a microscope slide or cover slip. The method of attaching the plate to the substrate must be very strong for pressure-driven flows because the pressure gradients, and hence the maximum pressures, can be very large. As an example, microchannels are often cast into the surface of blocks of polydimethylsiloxane (PDMS), a transparent flexible polymer commercially known as Sylgard. Closed channels are formed using a cover glass slip bonded to the PDMS surface by oxidizing both the surface of the PDMS replica and the glass by oxygen plasma treatment (70 W, 85 mTorr for 20 sec). When the two oxidized surfaces are brought into contact they bond covalently, creating a seal that can withstand up to 5 bars. Since the surfaces of the glass and the PDMS are each hydrophilic, filling the channels with aqueous liquids is relatively easy.

Most microfluidic channels have noncircular cross-sections whose shape is associated with the method of fabrication. Isotropic etching in glass or silicon produces cross-sections that are anywhere from semicircular

to rectangular with rounded corners in the bottom. Anisotropic etching in Si creates shapes defined by the crystallographic planes. A common case is Si with its <100> plane (Miller index) coincident with the planar surface to be machined. The <111> planes are inclined at 54.74° so that anisotropic etching creates either trapezoidal cross-sections with slanted sidewalls or triangular cross-sections. Laser machining of polymers creates roughly semicircular channels, while molding PDMS creates rectangular channels with slightly rounded corners. The various types of microfabrication and their characteristics are discussed in great detail throughout this handbook.

Fully developed flow in noncircular ducts is found by solving the Poisson Equation (10.10). Frequently, analytical solutions can also be found, but the numerical approach is so reliable that there is little need for exact solutions. Developing flow in the entrance region is more difficult, but here again numerical approaches are relatively straightforward. Table 10.2 summarizes the flow resistance for various laminar flows. One sees that the effect of the shape of the channel is relatively weak.

As mentioned earlier, a common approximation made in analyzing flow in ducts of noncircular cross-section is to use the results for circular ducts but replacing the hydraulic diameter of the noncircular duct with that of the round duct. For example, this can be done to estimate the flow resistance of fully developed flow and the resistance in the entrance region.
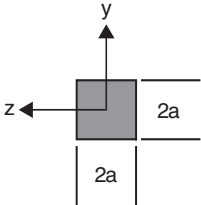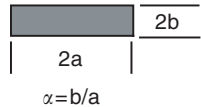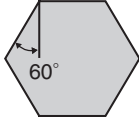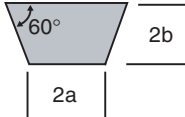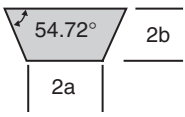
10.1.8   Experimental Studies of Flow Through Microchannels

Despite the fundamental simplicity of laminar flow in straight ducts, experimental studies of microscale flow have often failed to reveal the expected relationship between friction factor and Reynolds number. The frictional resistance of the flow has been reported, under *certain* conditions, to be *consistent* with predictions based on conventional macroscale Hagen-Poiseuille theory [Celata et al., 2002; Flockhart and Dhariwal, 1998; Jiang et al., 1995; Judy et al., 2002; Li et al., 2003; Liu and Garimella, 2004; Phares and Smedley, 2004; Sharp and Adrian, 2004; Wilding et al., 1994; Wu and Little, 1983], *increased* as compared to conventional macroscale predictions [Brutin and Tadrist, 2004; Celata et al., 2002; Cui et al., 2004; Hsieh et al.; 2004; Li et al., 2003; Mala and Li, 1999; Papautsky et al., 1999a, 1999b; Peng et al., 1994; Pfund et al., 2000; Phares and Smedley, 2004; Qu et al., 2000; Ren et al., 2001; Wu and Little, 1983] and *decreased* as compared to conventional macroscale predictions [Choi et al., 1991; Peng et al., 1994; Pfahler et al., 1990a, 1990b, 1991; Yu et al., 1995].

A brief summary is presented herein; for detailed historical summaries of the experiments that have been conducted to investigate the behavior of fluid flow in microchannels, see the recent reviews of microchannel fluid flows in both tabular [Sobhan and Garimella, 2001] and text format [Koo and Kleinstreuer, 2003; Obot, 2002]. Flow resistance experiments in microscale channels or tubes have been conducted over a large range of Reynolds numbers, geometries, and experimental conditions, and in the subsequent discussion of results, they will be grouped according to the results of friction factor measurements (follows macroscale predictions, higher than predictions, and lower than predictions).

The first experimental investigations of flow through microchannels in the early 1980s were motivated by the interest in high-performance heat sinking. The large surface-to-volume ratios of microchannels make them excellent candidates for efficient heat transfer devices. Tuckerman and Pease (1981) studied flow through an array of microchannels with approximately rectangular cross-sections (height range 50–56 μm, width range 287–320 μm). Although their study focused primarily on heat transfer characteristics, they "confirmed that the flow rate obeyed Poiseuille's equation." Shortly thereafter, a study of microchannels for use in small Joule-Thomson refrigerators was performed [Wu and Little, 1983]. Significant roughnesses were present in some of these etched silicon or glass channels, but friction factors measured in the smoothest channel showed reasonable agreement with theoretical macroscale predictions. A number of other experiments also have shown general agreement with the macroscale theoretical predictions for friction factor in the flow of a Newtonian fluid in at least certain parameter ranges in circular microtubes [Celata et al., 2002; Jiang et al., 1995; Judy et al., 2002; Li et al., 2003; Phares and Smedley, 2004; Sharp and Adrian, 2004], rectangular microchannels [Judy et al., 2002; Liu and Garimella, 2004], and channels with other cross-sectional shapes including the trapezoidal cross-section commonly

TABLE 10.2 Resistance to Flow in Fully Developed Flow Through Straight Microchannels of Various Cross-Sectional Geometry

Cross Section	f Re	u_{max}/u_B
$D = 2a$ (circle)	64	2.000
Square $2a \times 2a$	56.92	2.0962
Rectangle $2a \times 2b$, $\alpha = b/a$	$96[1 - 1.3553\alpha + 1.9467\alpha^2 - 1.7012\alpha^3 + 0.9564\alpha^4 - 0.2537\alpha^5]$	—
$\alpha \to 0$	96	1.5000
Hexagon $60°$	60	—
Trapezoid $60°$, $2b$ top, $2a$ height ($2b/2a$): 4.000	55.66	2.181
2.000	55.22	2.162
1.000	56.60	2.119
0.500	62.77	1.969
0.250	72.20	1.766
Trapezoid $54.72°$, $2b$ top, $2a$ height: 1.000	56.15	2.137

Data from Shah, R.K., and London, A.L. (1978) *Laminar Flow Forced Convection in Ducts,* Adv. in Heat Transfer series, Supp. 1, Academic Press, New York.

encountered in microfluidic applications due to anisotropic etching in the fabrication process [Flockhart and Dhariwal, 1998; Wilding et al., 1994].

In circular fused silica microchannels with diameters from approximately 50 to 250 μm and Reynolds numbers less than 1800, the results of more than 1500 measurements of pressure drop versus flow rate confirm agreement between macroscale Poiseuille theory and microscale measurements of the friction factor to within −1\% systematic and ±2.5% rms random error [Sharp and Adrian, 2004]. Similar agreement was also obtained using a 20% solution of glycerol and 1-propanol. Good agreement between conventional Poiseuille theory and experimental results has been reported for other microscale flows including: smooth circular microtubes with diameters of 80 to 200 microns [Li et al., 2003]; circular
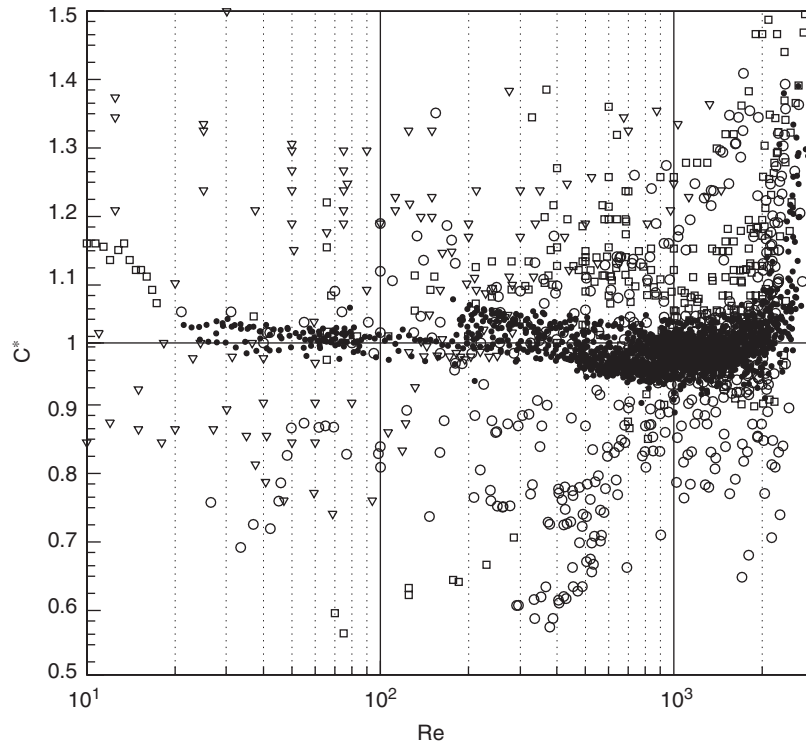
FIGURE 10.5   Comparison of C* vs. Reynolds number in the literature. Symbols indicate geometry of channel and the following data are shown: (·) circular microtubes, Sharp and Adrian (2004); ($\bigcirc$) circular microtubes, Yu et al. (1995), Choi et al. (1991), Judy et al. (2002), Mala and Li (1999); ($\triangledown$) trapezoidal microchannels, Pfahler et al. (1991), Flockhart and Dhariwal (1998), Wilding et al. (1994), Qu et al. (2000); ($\square$) rectangular microchannels, Pfahler et al. (1991), Pfahler et al. (1990b), Papautsky et al. (1999a), Pfund et al. (2000), Celata et al. (2002), Liu and Garimella (2004), Hsieh et al. (2004).

microtubes with diameters of 130 microns and Reynolds numbers less than 600 [Celata et al., 2002]; circular and square microtubes with diameter or hydraulic diameter of 15 to 150 microns and Reynolds numbers of 8–2300 [Judy et al., 2002]; smooth circular microtubes with diameters of 119 and 152 microns [Phares and Smedley, 2004]; and rectangular channels with hydraulic diameters from 244–974 microns [Liu and Garimella, 2004].

An increase in the frictional resistance of liquid flows in microchannels over theoretical predictions based on conventional macroscale theory has been reported in some studies [Brutin and Tadrist, 2004; Celata et al., 2002; Cui et al., 2004; Hsieh et al., 2004; Li et al., 2003; Mala and Li, 1999; Papautsky et al., 1999a, 1999b; Peng et al., 1994; Pfund et al., 2000; Phares and Smedley, 2004; Qu et al., 2000; Ren et al., 2001; Wu and Little, 1983], including increases of as much as 38% [Qu et al., 2002], 37% [Li et al., 2003], and 27% [Brutin and Tadrist, 2003] over conventional Poiseuille theoretical predictions. Another group of studies found the flow resistance to be less than theoretical macroscale predictions for certain conditions [Choi et al., 1991; Peng et al., 1994; Pfahler et al., 1990a, 1990b, 1991; and Yu et al., 1995].

To aid in comparing the results of these studies, a normalized friction factor C* is defined as

$$C^* = \frac{(f\,\mathrm{Re})_{\text{experimental}}}{(f\,\mathrm{Re})_{\text{theoretical}}}. \tag{10.28}$$

The wide variability of results is illustrated in Figure 10.5. There is also wide variability in experimental conditions, microchannel geometries, and methodology. The inconsistencies demonstrate the need for

both detailed velocity measurements and careful study of potential microscale effects such as surface roughness or electrical effects in order to conclusively understand the flow behavior in microscale channels.

10.1.9 Proposed Explanations for Measured Behavior

Thus far the explanations offered in the literature for anomalous behavior of friction factor and flow resistance in microchannels include surface/roughness effects and electrical charge, variations in viscosity, "early" transition to turbulence, entrance effects, inaccuracies in measuring channel dimensions, microrotational effects of individual fluid molecules, and geometry effects.

The increase in frictional resistance has often been reasonably linked to surface roughness. For example, in some studies [Li et al., 2003; Phares and Smedley, 2004; Wu and Little, 1983], experimental results on frictional resistance agreed well with Hagen-Poiseuille theory for smooth channels, but significant deviations were reported for flows through similar microchannels or tubes with increased surface roughnesses.

In macroscale theory, the surface roughness does not affect the flow resistance relationships in the laminar region [White, 1994]. Flow resistance results in microscale geometries have shown both a strong increase due to roughness [Li et al., 2003; Phares and Smedley, 2004; Wu and Little, 1983] and no effect due to roughness [Choi et al., 1991].

In terms of viscosity effects, a roughness viscosity model (RVM) has been proposed [Mala and Li, 1999, based on work by Merkle et al., 1974]. Assuming that surface roughness increases the momentum transfer near the wall, the roughness viscosity μ_r as a function of r is proposed to be higher near the wall and proportional to the Reynolds number [Mala and Li, 1999]. Implementing this roughness-viscosity model for water flowing through trapezoidal channels, reasonable agreement with model prediction and experimental results was found in most cases, but the model did not accurately depict the increased slope in the relationship between pressure drop and Reynolds number observed in the same experiments for $Re \geqslant 500$ [Qu et al., 2000]. Direct measurement of viscosity in very thin layers, or thin films, was performed by Israelachvili (1986). The viscosity of water was found to retain its bulk viscosity value to within 10% even in a film as thin as 5 nm. Concentrated and dilute NaCl/KCl solutions were also tested to assess the impact of double-layer forces on the value of viscosity near a surface. The viscosity of these dilute NaCl/KCl solutions remained only minimally affected until the last molecular layer near the wall. Based on these measurements, the viscosity of fluid in the wall region is not expected to vary significantly from the bulk value even in the presence of possible charging effects, somewhat contrary to the proposed explanations given by Mala and Li (1999) and Qu et al. (2000).

Other changes in viscosity are suggested to occur for liquids under extremely high pressure. A decrease in experimental flow rate for isopropanol and carbon tetrachloride as compared to conventional Hagen-Poiseuille theory has been reported and attributed to viscosity changes in isopropanol and carbon tetrachloride at pressures greater than 10 MPa, but in similar experiments any effects of high pressure on the viscosity of water could not be conclusively established [Cui et al., 2004]. It is also possible that the very high shear rates in these microchannels cause normally Newtonian fluids to behave in a non-Newtonian fashion. The shear rates in Sharp and Adrian (2004) were as high as $7.2 \times 10^5 \, \text{sec}^{-1}$. Measuring the rheology of fluids at very high shear rates is challenging. Using a flat plate rheometer, Novotny and Eckert (1974) determined that the relationship between shear stress and shear rate is still linear for water at a shear rate of 10,000 sec^{-1}, but the possibility that anomalous effects are caused by non-Newtonian behavior above shear rates of $10^4 \, \text{sec}^{-1}$ has not been adequately explored.

Electroviscous effects have been cited as a possible cause for increases in frictional resistance [Brutin and Tadrist, 2003; Ren et al., 2001]. Interestingly, while Brutin and Tadrist (2003) ruled out effects of surface roughness and attributed increases in resistance to ionic effects, Phares and Smedley (2004) ruled out electroviscous effects and indicate that surface roughness effects are a more likely explanation for departures from conventional Poiseuille theory.

Some dependence of flow resistance on channel geometry has been observed [Papautsky et al., 1999b; Peng et al., 1994; Pfahler et al., 1991; Qu et al., 2000]. One of the challenges of measuring the dependence

AQ7

AQ8

of flow resistance on aspect ratio or thinness of one dimension is the accurate characterization of the flow channels. Both Papautsky et al. (1999b) and Pfahler et al. (1991) acknowledge the difficulty of ensuring accurate size measurement and the corresponding difficulty of conclusively establishing a geometrical effect in their experiments. In at least one case, the departure from conventional macroscale theoretical predictions is found to depend on both Reynolds number and hydraulic diameter of the trapezoidal channels [Qu et al., 2000].

The critical Reynolds numbers for transition to turbulence in microchannel flows have been reported or modeled for certain flow conditions as below [Hsieh et al., 2004; Mala and Li, 1999; Morini, 2004; Peng et al., 1994; Pfund et al., 2000; Wu and Little, 1983] or consistent [Celata et al., 2002; Liu and Garimella, 2004; Sharp and Adrian, 2004] with nominal values for macroscale conduit flows, such as near 2000 for circular pipe flow [Darbyshire and Mullin, 1995]. The ranges of critical Reynolds numbers cited in the literature include values both dramatically lower than the nominal macroscale values, such as 240 [Hsieh et al., 2004], 200–700 [Peng et al., 1994], 400 [Wu and Little, 1983], 300–900 [Mala and Li, 1999], and values slightly lower than nominal macroscale values [Pfund et al., 2000]. Conclusive causes of observed early transition to turbulence have not been established, but the reported trend in the most recent experiments, Hsieh et al.'s (2004) work not withstanding, has been that transition is occurring at critical Reynolds numbers consistent with those in macroscale experiments. In earlier experiments and in Hsieh et al.'s (2004) experiments, the early-transition observations were based primarily on data obtained from bulk flow measurements. More recently the transitional Reynolds number range was established using flow visualization [Liu and Garimella, 2004; Hsieh et al., 2004] and by quantifying the magnitude of spatial and temporal velocity variations measured using micro-Particle Image Velocimetry [Sharp and Adrian, 2004]. Reports of irregular tracer motion are used to justify the conclusion that transition is occurring at Reynolds numbers lower than Re $\sim$ 470 in Hsieh et al. (2004); in contrast, the spatial and temporal velocity variations indicated an onset of transition for Reynolds numbers of 1800–2000 in circular microtubes [Sharp and Adrian, 2004], and flow visualization indicated an onset of transition at Reynolds numbers of approximately 1800–2200 in rectangular channels [Liu and Garimella, 2003] consistent with nominal critical Reynolds numbers of 2000–3000 in macroscale rectangular conduits, where the critical Reynolds number in a rectangular channel can depend on aspect ratio [Hanks and Ruo, 1966].

Certainly, the inclusion or exclusion of entrance effects can affect the magnitude of the measured friction factor and is generally considered in careful experimental studies. Regardless of the geometry, to accurately measure the dimensions of these microchannels is extremely difficult, particularly when one of the dimensions is on the order of a couple of microns. The pressure drop in a round capillary is

AQ9

inversely proportional to D^4 (Equation [10.21]), so an inaccuracy of 5% in measuring D can bias resistance results by 20%, enough to explain the majority of the early discrepancies between the conventional macroscopic resistance predictions and the observed values in Figure 10.5.

The validity of the no-slip assumption for liquids in contact with a solid surface has also been brought into question [Choi et al., 2003; Tretheway and Meinhart, 2002; 2004; Zhu and Granick, 2001], particularly in the case of coated microchannels. Documented slip lengths are at most 1 mm [Tretheway and Meinhart, 2002] and as low as tens of nm [Choi et al., 2003] and could be an additional source of error in flow resistance experiments. For a detailed discussion of fluid slip, refer to the chapter "Slip Behavior

AQ10

in Simple and Polymeric Fluids" in this handbook.

The details of other models incorporating micropolar fluid theory, cross-sectional geometry, roughness, entrance, and viscous dissipation effects may be found in the literature [Koo and Kleinstreuer, 2003; Morini, 2004; Papautsky, et al. 1999a].

10.1.10 Measurements of Velocity in Microchannels

Along with the growth of research in microdevices, rapid development of experimental techniques for investigating flows in such devices is also underway including modification of experimental techniques commonly applied at the macroscale and development of new techniques. Measurements of velocities in

microchannels have been obtained using bulk flow, pointwise, and field measurements. Each technique has certain advantages that may make it more suitable to providing a specific type of flow field information. A brief summary is included herein. For more detailed discussions of diagnostic techniques, including the most recent advances in acquisition and processing techniques, see the chapter in this handbook entitled "Diagnostic Tools for Microfluidics," Nguyen and Wereley (2002, chap. 4), and Devasenathipathy et al. (2003).

The majority of flow resistance data in microscale geometries to date has been obtained through the use of bulk flow measurements. Typical methods used to measure bulk flow rate, include an in-line flowmeter or the timed collection of fluid at the outlet and pressure taps located at the inlet and outlet or simply at the inlet if the pressure at the outlet is known. Bulk flow measurements require neither optical access to the microchannel nor seeding, and there are no restrictions on the geometrical parameters of the channel. However, given the disagreement in results regarding microscale effects on flow resistance in particular, bulk flow measurements lack sufficient detail to discern potential mechanisms causing deviation from macroscale theory. Detailed measurements of flow velocity are also useful for optimizing the design of complex microdevices for mixing, separation, reaction, and thermal control. For examples of these devices, consult the section on applications of MEMS in this handbook.

The first micro-Particle Image Velocimetry (micro-PIV) measurements were made in a Hele-Shaw cell [Santiago et al., 1998]. These velocity field measurements were resolved to 6.9 μm in the lateral directions and 1.5 μm in the depth direction and demonstrated the applicability of the well-established PIV technique for microflows. Micro-PIV measurements in a rectangular glass microchannel with 200 nm fluorescent tracer particles (Re < 1) have been described in Meinhart et al. (1999). With improved acquisition and analysis, the lateral resolution was 13.6 μm in the streamwise direction significantly better 0.9 μm in the cross-stream direction, the direction of highest velocity variation. The first demonstration of micro-PIV within a circular capillary was performed in a 236 μm diameter channel with Reynolds number ≪ 1 [Koutsiaris et al., 1999]. The seeding particles were 10 μm glass spheres, and the resolution of the measurements was 26.2 μm in the cross-stream direction. The measured velocity profiles agreed well with the predicted laminar parabolic profiles. More recently, micro-PIV has been used to study the velocity profiles and turbulence statistics of water flows in circular channels with $D \sim$ 100–250 μm and Reynolds numbers up to 3000 using 2 μm fluorescent particles [Sharp and Adrian, 2004].

Alternate visual methods applied to microchannel velocity measurements have been demonstrated by numerous researchers [Brody et al., 1996; Maynes and Webb, 2002; Ovryn, 1999; Paul et al., 1998b; Taylor and Yeung, 1993]. Molecular tagging velocimetry (MTV) was adapted to the microscale, and velocity profiles were obtained in circular tubes with $D = 705$ μm, and for Re = 600–5000 [Maynes and Webb, 2002]. The spatial resolution of these measurements was approximately 10 μm. The measured velocity profiles were consistent with macroscale laminar predictions for Re ≤ 2000 and show indications of transition at a Reynolds number of approximately 2100. Relevant development issues for microscale MTV are similar to those for PIV, namely optical access and index of refraction compensation, particularly for curved surfaces, and optimized detection of the tracking particles (PIV) or beams (MTV).

Particle tracking, streak quantification, or dye visualization can be implemented given optical access and the ability to illuminate the flow [Brody et al., 1996; Devasenathipathy et al., 2002: Taylor and Yeung, 1993]. Care must be exercised in the extraction of quantitative data, particularly if there is a large depth of field of the imaging device or optical complications due to complex microchannel geometries or if the particles or molecules are not accurately following the flow due to charge, size, or density effects.

Novel three-dimensional measurement techniques for microchannel flows are currently in development [Hitt and Lowe, 1999; Ovryn, 1999]. Building upon a technique already developed for the study of microscale structures, Hitt and Lowe (1999) used confocal imaging to build a three-dimensional map of the *separation surface* following a bifurcation, where the separation surface describes the interfacial boundary between two components from different branches of the bifurcation. Using two laser-scanning confocal microscopes, a series of thin (4.5 or 7.1 μm) horizontal slices were acquired and reconstruction software was used to combine these slices into a three-dimensional map. Again, optical access and effects are primary issues in the implementation of this method, and it is not suitable for unsteady flows. Ovryn

(1999) sought to resolve and interpret the scattering pattern of a particle to determine its three-dimensional position, and has applied this technique to laminar flow.

X-ray imaging techniques do not require optical access in the channel, though a contrast medium detectable by x-rays must be used as the working fluid. Lanzillotto et al. (1996) obtained flow displacement information from microradiograph images of emulsion flow through a 640 μm diameter tube and iododecane flow through a silicon V-groove chip.

The level of complexity increases when electrokinetic flows are considered. A few of the earliest visual measurements of electrokinetic flows are described in Paul et al. (1998b); Cummings (1999); and Taylor and Yeung (1993). Paul et al. (1998b) seeded the flow with an uncaged fluorescent dye. Once the dye was uncaged by an initial UV laser pulse, the flow was illuminated by succeeding pulses of blue light for CCD image acquisition, causing the excitation of only the uncaged dye molecules. This technique was applied to both pressure-driven and electrokinetic flows in circular capillaries with diameters of the order 100 μm. Since the dye transport represents represented both convection and diffusion, requisite care is necessary to separate the effects [Paul et al., 1998b]. This method can be used also to acquire quantitative information regarding diffusion effects. More recently, particle tracking techniques have been adapted to electrokinetic flows [Devasenathipathy et al., 2002].

Pointwise techniques were used to acquire early velocity measurements in microfluidic systems [Chen et al., 1997; Tieu et al., 1995; Yazdanfar et al., 1997]. Optical doppler tomography combines elements of Doppler velocimetry with optical coherence tomography in an effort to develop a system that can quantify the flow in biological tissues [Chen et al., 1997]. Chen et al. (1997) applied the technique to a 580 μm diameter conduit seeded with 1.7 μm particles. An approximate parabolic profile was measured in the first test, and in the second test, it was shown that fluid particle velocities could be measured even with the conduit submerged in a highly scattering medium, as would be the case for particles in biological tissues. A similar measurement technique has been used for in vivo measurements [Yazdanfar et al., 1997]. An adaptation of laser doppler anemometry (LDA) techniques to microscale flows was demonstrated by Tieu et al. (1995), and pointwise data were obtained in a 175 μm channel.

10.1.11   Non-Linear Channels

For practical MEMS applications, it is often useful to consider mixing or separation of components in microchannels. Numerous designs have been proposed, including T- and H-shaped channels, zigzag shaped channels, 2-D and 3-D serpentine channels, and multilaminators.

For example, Weigl and Yager (1999) have designed a T-sensor for implementation of assays in microchannels, as shown in Figure 10.6. A reference stream, a detection stream, and a sample stream have been introduced through multiple T-junctions into a common channel. The design relied upon the differential diffusion of different sized molecules to separate components in the sample stream. Differential diffusion rates are also fundamental to the design of the H-filter, used to separate components [Schulte et al., 2000]. Application of a slightly different T-channel design has been demonstrated for measurement of diffusion coefficients of a species in a complex fluid [Galambos and Forster, 1998].

A layering approach has been implemented by Branebjerg et al. (1996), splitting the streams and relayering to increase interfacial area, thus promoting mixing. Adding complexity to the flow field also has potential to increase the amount of mixing between streams, as demonstrated by Branebjerg et al.'s (1995) zigzag channel and the serpentine channels introduced by Liu et al. (2000). The 3-D serpentine channel in Liu et al. (2000) was designed to introduce chaotic advection into the system and further enhance mixing over a 2-D serpentine channel. A schematic of the 3-D serpentine channel is shown in Figure 10.7.

For further information on the use of nonlinear channels in microdevices, consult the applications of MEMS section of this handbook.

10.1.12   Capacitive Effects

While liquids are incompressible, the systems through which they flow may expand or contract in response to pressure in the liquid. This behavior can be described by analogy to flow in electrical circuits.
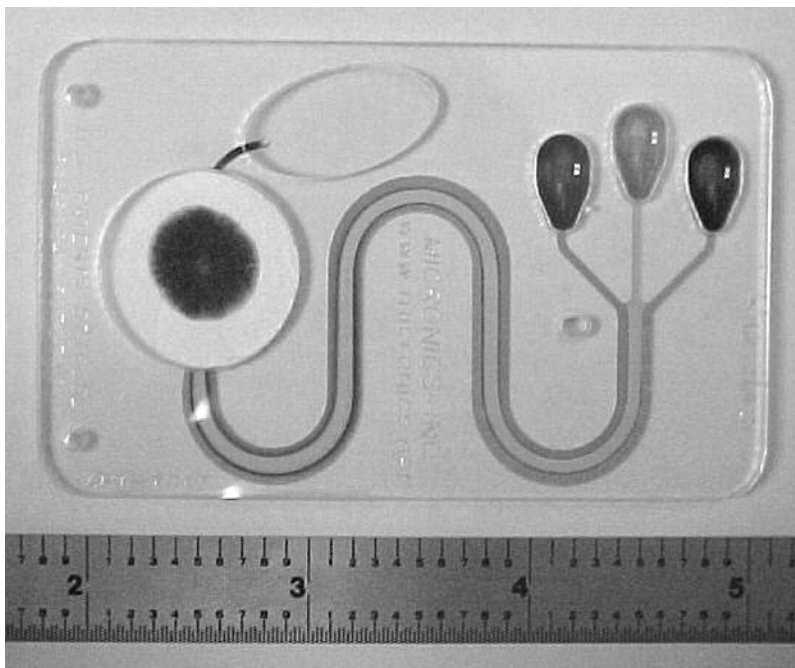
FIGURE 10.6   T-Sensor, self-calibrating microchemical reactor and sensor. This design allows for self-calibration through the simultaneous flow of a reference solution on the opposite flank of the indicator stream from the sample to be analyzed. (Reprinted with permission from Micronics, Inc., Redmond, WA, 2000.).

AQ38
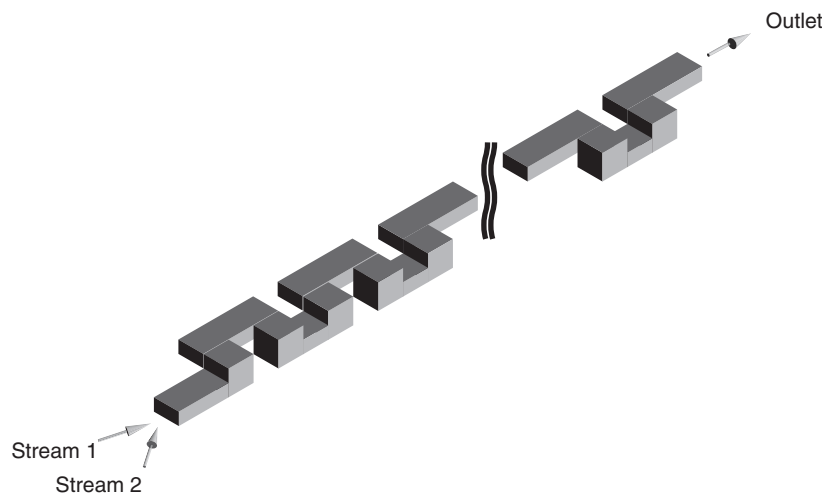
FIGURE 10.7   Three-dimensional serpentine channel. (Reprinted with permission from Liu et al. [2000], personal communication.)

In this analogy, fluid pressure corresponds to electrical voltage $p \sim V$; the volume flow rate corresponds to electrical current $Q \sim I$; and the flow resistance through a fluid element corresponds to an electrical resistor $R_{\text{flow}} \sim R_{\text{elec.}}$. Thus for capillary flow, $\Delta p = R_{\text{flow}}Q$, where $R_{\text{flow}} = 8\,\mu L/\pi a^4$ (c.f., Equation [21]), whereas in the electrical analogy, $\Delta V = R_{\text{elec}}I$. If a fluid element is able to change its volume (expansion of plastic tubing, flexing in pressure transducer diaphragm, etc.), fluid continuity implies that:

AQ14

$$\Delta Q = C_{\text{flow}} \frac{dp}{dt} \qquad\qquad (10.29)$$

where C_{flow} is the capacitance of the fluid element. The corresponding electrical law is $I = C_{elec}\, dV/dt$, where C_{elec} is the electrical capacitance.

It is well known in the context of electrical circuits that a resistor and capacitor in combination cause transients whose time constant τ is proportional to $R_{elec}C_{elec}$. In a microfluidic circuit, any capacitive element in combination with a flow resistance leads to analogous transients whose time constant is proportional to $R_{flow}C_{flow}$. Since R_{flow} can be very large in microchannels, the time constant can be surprisingly large, that is 10^3 seconds. Consequently, capacitive effects can cause significant and inconveniently long transients.

10.1.13 Applications of Particle/Cell Manipulation in Microfluidics

A number of research efforts are underway to develop particle separation, sorting, and detection capabilities in microfluidic networks with a particular emphasis on biological applications [Berger et al., 2001; Blankenstein and Larsen, 1998; Cho and Kim, 2003; Chou et al., 2000; Glückstad, 2004; Lee et al., 2001, 2003; Mirowski et al., 2004]. Cell or particle separation and sorting techniques have been proposed using concepts from electrokinetics [Cho and Kim, 2003; Fu et al., 2004], optical methods [Glückstad, 2004], magnetics [Mirowski et al., 2004; Berger et al., 2001], and hydrodynamic-based manipulation [Blankenstein and Larsen, 1998; Chou et al., 2000; Lee et al., 2001, 2003].

10.1.14 Recommended Review Papers on Microfluidics

For further information on research and development trends in microfluidics, referred to two review papers, Stone et al. (2004) and Ho and Tai (1998).

10.2   Electrokinetics Background

The first demonstration of electrokinetic phenomena is attributed to F.F. Reuss, who demonstrated electroosmotic flow of water through a clay column in a paper published in the Proceedings of the Imperial Society of Naturalists of Moscow in 1809 [Probstein, 1994]. In the latter part of the 20th century, the main applications of electrokinetic phenomena have been fairly wide-ranging from the dewatering of soils and waste sludges using electric fields [Hiemenz and Rajagopalan, 1997] to the study of the stability of colloidal suspensions for household paint and to devices that use electrophoretic mass transfer of colloidal suspensions to produce images on a planar substrate [Kitahara and Watanabe, 1984]. A community that has paid particular attention to the study of mass and momentum transport using electrokinetic effects is the developers of capillary electrophoresis (CE) devices [Khaledi, 1998; Landers, 1994; Manz et al., 1994]. CE devices are used to separate biological and chemical species by their electrophoretic mobility, which is roughly proportional to their mass-to-charge ratio. CE devices that employ a sieving matrix separate macromolecules based on size (e.g., DNA separations or surfactant-coated, denatured protein separations). These traditional CE systems incorporate on-line detection schemes such as ultraviolet radiation scatter/absorption and laser-induced fluorescence [Baker, 1995; Landers, 1994].

Electrokinetics is the general term describing phenomena that involve the interaction between solid surfaces, ionic solutions, and macroscopic electric fields. Two important classes of electrokinetics are electrophoresis and electroosmosis where the motions of particles and electrolyte liquids, respectively, occur when an external electric field is applied to the system. Electrophoresis is the induced drift motion of colloidal particles or molecules suspended in liquids that results from the application of an electric field. Electroosmosis describes the motion of electrolyte liquids with respect to a fixed wall that results when an electric field is applied parallel to the surface. An example of electroosmosis is the liquid pumping that occurs in a microcapillary when an electric field is applied along the axis of the capillary [Hunter, 1981; Levich, 1962; Probstein, 1994]. Two other phenomena also classified under electrokinetics are flows with a finite streaming potential and sedimentation potential. These phenomena are counter-examples of electroosmosis and electrophoresis respectively. Streaming potential is the spontaneous generation of an

electric potential from a pressure-driven flow in a charged microchannel [Hunter, 1981; Scales et al., 1992]. Sedimentation potential is the generation of an electric potential that results from the sedimentation (e.g., due to gravity) of a charged particle [Russel et al., 1999]. All of the phenomena classified under the term electrokinetics are manifestations of the electrostatic component of the Lorentz force (on ions and surface charges) and Newton's second law of motion. These interactions between charged particles and electric fields often involve electric double layers formed at liquid/solid interfaces, and an introduction to this phenomenon is presented below. Electrokinetic flows are in general a subclass of electrohydrodynamic flows [Melcher, 1981; Saville, 1997], which describe the general coupling between electric fields and fluid flow. Electrokinetic systems are distinguishable in that they involve liquid electrolyte solutions and the presence of electrical double layers (i.e., involve electrophoresis and electroosmosis).

10.2.1   Electrical Double Layers

Most solid surfaces acquire a surface electric charge when brought into contact with an electrolyte (liquid). Mechanisms for the spontaneous charging of surface layers include the differential adsorption of ions from an electrolyte onto solid surfaces (e.g., by ionic surfactants), the differential solution of ions from the surface to the electrolyte, and the deprotonation/ionization of surface groups [Hunter, 1981]. The most common of these in microfluidic electrokinetic systems is the deprotonation of surface groups on the surface of materials like silica, glass, acrylic, and polyester. In the case of glass and silica, the deprotonation of surface silanol groups (SiOH) determines the generated surface charge density. The magnitude of the net surface charge density at the liquid/solid interface is a function of the local pH. The equilibrium reaction associated with this deprotonation can be represented as

$$SiOH \Leftrightarrow SiO^- + H^+ \tag{10.30}$$
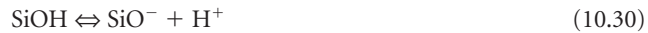
Models describing this reaction have been proposed for several types of glass and silica [Hayes et al., 1993; Huang et al., 1993; Scales et al., 1992]. In practice, the full deprotonation of the glass surface, and therefore the maximum electroosmotic flow mobility, is achieved for pH values greater than about 9.

In response to the surface charge generated at a liquid–solid interface, nearby ions of opposite charge in the electrolyte are attracted by the electric field produced by the surface charge, and ions of like charge are repelled. The spontaneously formed surface charge therefore forms a region near the surface called an electrical double layer (EDL) that supports a net excess of mobile ions with a charge opposite to that of the wall. Figure 10.8 shows a schematic of the EDL for a negatively charged wall (e.g., as in the case of a glass surface). The region of excess charge formed by the counterions shielding the wall's electric field can be used to impart a force on the bulk fluid through ion drag.

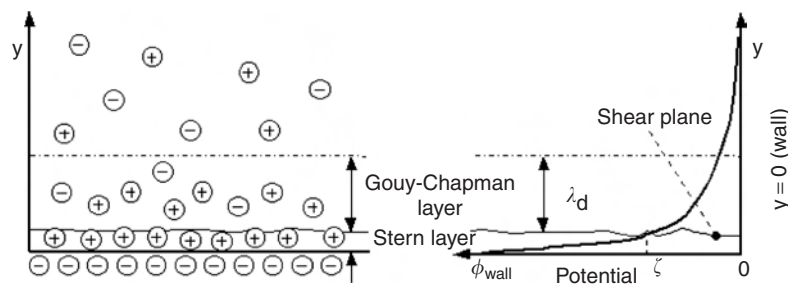**FIGURE 10.8**   Schematic of the electrical double layer (EDL): (a) Distribution of co- and counterions near a charged wall. The Stern and Gouy-Chapman layers are shown with the Gouy-Chapman thickness roughly approximated as the Debye length of the solution. (b) A plot of the negative potential distribution near a glass wall indicating the zeta potential, the wall potential, and the location of the shear plane.

As shown in Figure 10.8, counterions reside in two regions divided into the Stern and Gouy-Chapman diffuse layers [Adamson and Gast, 1997; Hunter, 1981]. The Stern layer counterions are adsorbed onto the wall, while the ions of the Gouy-Chapman diffuse layer are free to diffuse into the bulk fluid and therefore available to impart work on the fluid. The plane separating the Stern and Gouy-Chapman layers is called the shear plane. The bulk liquid far from the wall is assumed to have net neutral charge. Also in Figure 10.8 is a sketch of the potential associated with the EDL. The magnitude of the potential is a maximum at the wall and drops rapidly through the Stern layer. The potential at the shear plane, which is also the boundary of the liquid flow problem, is called the "zeta potential" ζ Because of the difficulties associated with predicting the properties of the EDL from first principles [Hunter, 1981], the zeta potential is typically viewed as an empirical parameter determined using electroosmotic or streaming potential flow measurements.

A simple treatment of the physics of the diffuse portion of the EDL is presented here; it assumes a liquid with constant properties (i.e., constant viscosity and electrical permittivity). A more detailed model of the diffuse portion of the electrical double layer should include non-continuum effects such as finite-ion size effects and gradients in the dielectric strength and viscosity of the fluid [Hunter, 1981]. The width of the diffuse portion of the EDL is determined by the opposing forces of electrostatic attraction and thermal diffusion. This balance between electromigration and diffusive fluxes, together with the Nernst-Einstein equation relating ion diffusivity and mobility [Hiemenz and Rajagopalan, 1997], can be used to show that the concentration profile is described by a Boltzmann distribution. For an EDL on a flat plate, the Boltzmann distribution of ions of species i, c_i, is

$$c_i(y) = c_{\infty,i} \exp\left(-\frac{ze\phi(y)}{kT}\right), \tag{10.31}$$

where $c_{\infty,i}$ is the molar concentration of ion i in the bulk, z is the valance number of the ion, ϕ is the local potential, T is temperature, e is the charge of an electron, and k is Boltzmann's constant. The coordinate y is perpendicular to the wall and the origin is at the shear plane of the EDL. The net charge density in the EDL, ρ_E, is related to the molar concentrations of N species using the relation

$$\rho_E = F\sum_{i=1}^{N} z_i c_i, \tag{10.32}$$

where F is Faraday's constant. The net charge density can also be related to the local potential in the diffuse EDL by the Poisson equation

$$\nabla^2\phi = -\frac{\rho_E}{\varepsilon} \tag{10.33}$$

where ε is the permittivity of the liquid. Substituting Equations (10.31) and (10.32) into Equation (10.33), we find that

$$\frac{d^2\phi}{dy^2} = \frac{-F}{\varepsilon}\sum_{i=1}^{N} z_i c_{\infty,i} \exp\left(-\frac{ze\phi(y)}{kT}\right) \tag{10.34}$$

For the simple case of a symmetric electrolyte with (two) monovalent ions, this relation becomes

$$\frac{d^2\phi}{dy^2} = \frac{2Fz_i c_\infty}{\varepsilon}\sinh\left(\frac{ze\phi(y)}{kT}\right) \tag{10.35}$$

where c_∞ is the molar concentration of each of the two ion species in the bulk. This relation is the nonlinear Poisson-Boltzmann equation. A closed form, analytical solution of this equation for the EDL on a flat wall is given by Adamson and Gast (1997) and Hunter (1981).

A well-known approximation to the Poisson-Boltzmann solution known as the Debye-Huckle limit is the case where the potential energy of ions in the EDL is small compared to their thermal energy so that the argument of the hyperbolic sine function in Equation (10.35) is small. Applying this approximation, Equation (10.35) becomes

$$\frac{d^2\phi}{dy^2} = \frac{\phi(y)}{\lambda_D^2} \tag{10.36}$$

where λ_D is the Debye length of the electrolyte defined as

$$\lambda_D \equiv \left(\frac{\varepsilon k T}{2 z^2 \, F^2 \, c_\infty} \right)^{\frac{1}{2}} \tag{10.37}$$

for a symmetric monovalent electrolyte. The Debye length describes the characteristic thickness of the EDL, which varies inversely with the square root of ion molar concentration. At typical biochemical, singly ionized buffer concentrations of 10 mM, the thickness of the EDL is therefore on the order of a few nanometers [Hiemenz and Rajagopalan, 1997]. In analyzing electrokinetic flow in microchannels, the Debye length should be compared to the characteristic dimension of the microchannel in order to classify the pertinent flow regime. Overbeek (1952) points out that the Debye-Huckle approximation of the potential of the EDL holds remarkably well for values of the ratio $ze\phi/(kT)$ up to approximately 2. This value is equivalent to a zeta potential of about 50 mV, which is within the typical range of microfluidic applications.

Models of the physics of the EDLs can be used to extrapolate zeta potential of particles and microchannels across a significant range of buffer concentration, fluid viscosity, electrical permittivity of electrolytes, and field strengths given only a few measurements. One of the most difficult zeta potential extrapolations to make is across different values of pH because pH changes the equilibrium reactions associated with the charge at the liquid–solid interface.

A full formulation of the coupled system of equations describing electroosmotic and electrokinetic flow includes the convective diffusion equations for each of the charged species in the system, the Poisson equation for both the applied electric field and the potential of the EDL, and the equations of fluid motion. A few solutions to this transport problem relevant to microfluidic systems are presented below.

10.2.2 EOF with Finite EDL

Electroosmotic flow (EOF) results when an electric field is applied through a liquid-filled microchannel having an EDL at the channel surfaces, as described above. This applied electric field introduces an electrostatic Lorentz body force

$$\rho \mathbf{b} = \rho_E \mathbf{E} \tag{10.38}$$

into the equation of motion for the fluid, Equation (10.3). Within the EDL, the electric field exerts a net force on the liquid causing the liquid near the walls to move. Alternately, one can describe the effect as simply the ion drag on the liquid associated with the electrophoresis of the ions in the EDL. The fluid in the EDL exerts a viscous force on the rest of the (net zero charge) liquid in the bulk of the channel. For EDLs much smaller than the channel dimension D, the fluid velocity reaches steady state in a short time t that is on the order of D^2/v, where v is kinematic viscosity of the fluid. The resulting bulk electroosmotic flow is depicted schematically in Figure 10.9.

The equation of motion for steady low-Reynolds-number flow in the microchannel is given by Equation (10.39).

$$\nabla p = \mu \nabla^2 \mathbf{u} + \rho_E \mathbf{E} \tag{10.39}$$

Substituting Equation (10.33) for the charge density, results in

$$\nabla^2 \left(\mathbf{u} - \frac{\varepsilon \mathbf{E}}{\mu} \phi \right) = \frac{\nabla p}{\mu}. \tag{10.40}$$

In Equation (10.40), the electric field, $\mathbf{E}$, can be brought into the Laplace operator because $\nabla \cdot \mathbf{E} = \nabla \times \mathbf{E} = 0$. Equation (10.40) is linear so that the velocities caused by the pressure gradient and the electric field can be considered separately and then superposed as follows:

$$\nabla^2 \left(\mathbf{u}_{\text{EOF}} - \frac{\varepsilon \mathbf{E}}{\mu} \phi \right) = 0, \tag{10.41}$$
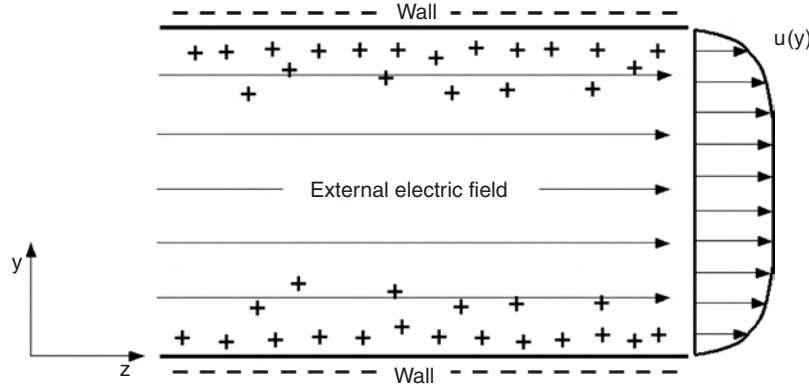
FIGURE 10.9 Schematic of an electroosmotic flow channel with a finite EDL. The charges drawn in the figure indicate net charge. The boundary layers on either wall have a thickness on the order the Debye length of the solution. For non-overlapping EDLs, the region near the center of the channel is net neutral.
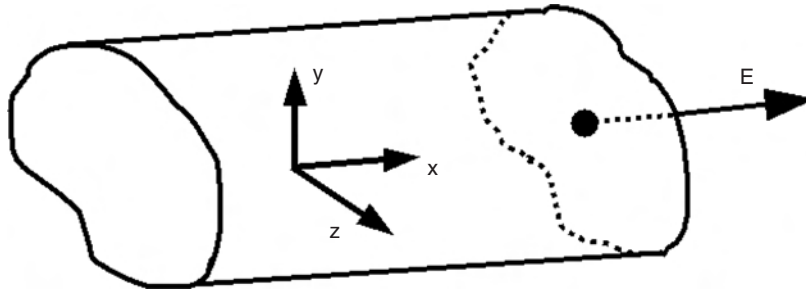

FIGURE 10.10 Section of a long, straight channel having an arbitrary cross-section.

$$\nabla^2 \mathbf{u}_{\text{pressure}} = \frac{\nabla p}{\mu}. \tag{10.42}$$

Together with Equation (10.2), these are the general equations for electroosmotic flow in a microchannel. Evaluation of the pressure-driven flow component of velocity in a microchannel can leverage analytical solutions available for channels of various cross-sections [White, 1991]. The pressure gradient can be applied externally or may arise internally because of variations in the zeta potential at the channel walls [Anderson and Idol, 1985; Herr et al., 2000].

Now consider electroosmosis in a long straight microchannel with a finite width electrical double layer and an arbitrary cross-section that remains constant along the flow direction (*x*-axis), as shown in Figure 10.10. The applied electric field is assumed to be uniform and along the *x*-axis of the microchannel. For the case where the potential at the wall is uniform, the solution to Equation (10.41) is

$$u_{\text{EOF}} - \frac{\varepsilon E \zeta}{\mu} \phi = \frac{-\varepsilon E \zeta}{\mu}, \tag{10.43}$$

with the zeta-potential ζ, being the value of ϕ at the top of the double layer. In Equation (10.43) u_{EOF} and *E* are the unidirectional velocity and unidirectional applied electric field respectively. The general expression for the electroosmotic velocity, implicit in the potential is then

$$u_{\text{EOF}}(y, z) = \frac{-\varepsilon E \zeta}{\mu} \left(1 - \frac{\phi(y,z)}{\zeta} \right). \tag{10.44}$$
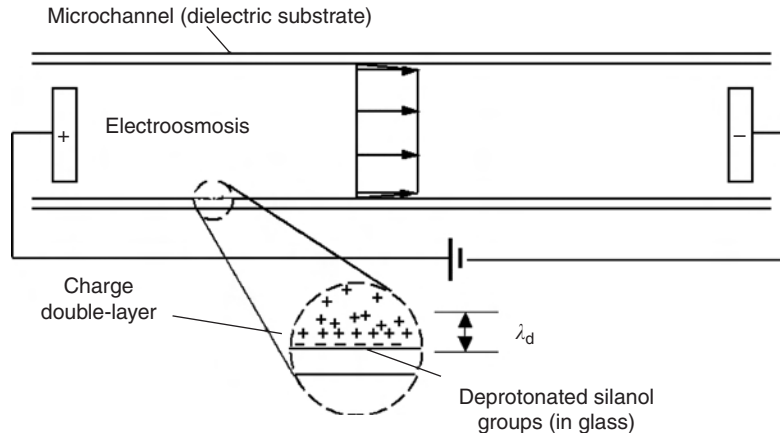
FIGURE 10.11 Schematic of electroosmotic flow in a glass microchannel with a thin EDL. A zero pressure gradient plug flow is shown. The electrodes on the ends of the channel indicate the polarity of the electric field.

To compute values for the velocity given in Equation (10.44), an expression for the potential $\phi(y, z)$ is required. In general $\phi(y, z)$ can be computed numerically from Equation (10.34), but analytical solutions exist for several geometries. Using the Boltzmann equation for a symmetric analyte and the Debye-Huckel approximation discussed in the previous section, Rice and Whitehead (1965) give the solution for electroosmosis in a long cylindrical capillary.

$$u_{\text{EOF}}(r) = \frac{-\varepsilon E \zeta}{\mu}\left(1 - \frac{I_o(r/\lambda_D)}{I_o(r/a)}\right). \tag{10.45}$$

In Equation (10.45), I_o is the zero-order modified Bessel function of the first kind; r is the radial direction; and a is the radius of the cylindrical capillary. This solution can be superposed with the solution of Equation (10.42) for a constant pressure gradient. The resulting composite solution is

$$u(r) = \frac{-\varepsilon E \zeta}{\mu}\left(1 - \frac{I_o(r/\lambda_D)}{I_o(r/a)}\right) - \frac{dp}{dx}\frac{a^2}{4\mu}\left(1 - \frac{r^2}{a^2}\right). \tag{10.46}$$

Burgeen and Nakache (1964) give a general solution for electroosmotic flow between two long, parallel plates, for a finite EDL thickness (but with nonoverlapping EDLs). For other more complex geometries and many unsteady problems, numerical solutions for the electroosmotic flow are required [Arulanandam and Li, 2000; Bianchi et al., 2000; Dutta et al., 2002; Myung-Suk and Kwak, 2003; Patankar and Hu, 1998; Yao, 2003a].

However, when the Debye length is finite but much smaller than other dimensions (e.g., the width of the microchannel) the disparate length scales can make numerical solutions difficult [Bianchi et al., 2000; Patankar and Hu, 1998]. In many cases, EOF in complex geometries can be determined numerically using a thin double layer assumption described in the next section.

10.2.3 Thin EDL Electroosmotic Flow

This section presents a brief analysis of electroosmotic flow in microchannels with thin EDLs. Figure 10.11 shows a schematic of an electroosmotic flow in a microchannel with zero pressure gradient. As shown in the figure, the Debye length of typical electrolytes used in microfabricated electrokinetic systems is much smaller than the hydraulic diameter of the channels. Typical Debye-length–to–channel diameter ratios are less than 10^{-4}. For low Reynolds number electroosmotic flow in a cylindrical channel in the presence

of a constant axial pressure gradient and a Debye length much smaller than the capillary radius, the solution of the velocity field is simply

$$u(r) = -\frac{\varepsilon \zeta E}{\mu} - \frac{dp}{dx}\frac{(a^2 - r^2)}{4\mu}.$$ (10.47)

This equation can be derived by evaluating Equation (10.46) in the limit of a thin EDL (i.e., a small value of λ_D/a).

The zeta potential typically determines flow velocities and flow rates in common thin EDL systems. As mentioned above, this quantity can often be interpreted as an empirically measured mobility parameter that determines the local velocity of the flow at the top of the electrical double layer. The zeta potential can be approximately related to the local surface charge density on the wall and the bulk fluid properties by applying continuum field and flow theory. Theoretically, the zeta potential is defined as the value of the electrostatic potential at the plane that separates double layer counterions that are mobile from those that are fixed. For the case of zero applied pressure gradients, Equation (10.47) reduces to the well-known AQ15 Helmholtz-Smoulochowski relation for electroosmotic flow: $u = \varepsilon \zeta E/\mu$ [Probstein, 1994]. Other thin EDL solutions include that of Ghosal (2002) for slowly varying zeta potential and cross-sectional area channels, and Oddy and Santiago (2004) for a rectangular channel with four different wall zeta potentials and an applied AC electric field.

10.2.4 Electrophoresis

Many electrokinetic microfluidic systems leverage the combination of electroosmotic and electrophoresis to achieve biological separations and to transport charged particles (e.g., biological assay microbeads) and ions. Because of this, we present here a short introduction to electrophoresis. Electrophoresis is the induced drift motion of colloidal particles or molecules suspended in polar solutions that results from the application of an electric field. Two important regimes of electrophoresis depicted in Figure 10.12 are for the electromigration of species that that are either large or small compared to the Debye length of the ionic solution in which they are suspended.

Electrophoresis of ionic molecules and macromolecules can be described as a simple balance between the electrostatic force on the molecule and the viscous drag associated with its resulting motion. As a result, the electrophoretic mobility (velocity-to-electric field ratio) of molecules is a function of the molecule's size/molecular weight and directly proportional to their valence number or

$$u = \frac{qE}{3\pi\mu d}(d \ll \lambda_d)$$ (10.48)

Electrophoresis of an ion

Electrophoresis of a microsphere
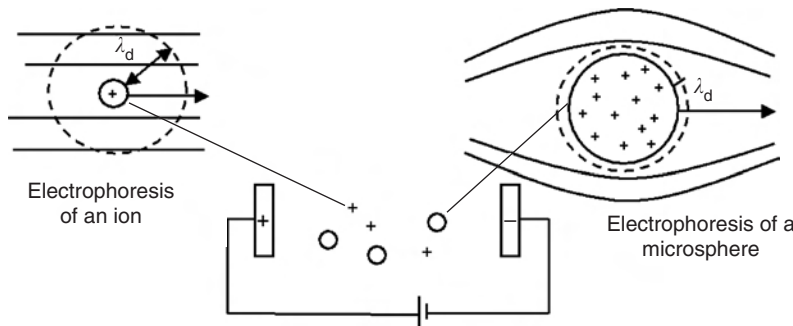
FIGURE 10.12 Two limiting limits of electrophoresis in an electrolyte. Shown are electrophoretic particles in the electric field generated between two electrodes. On the left is the detail of a charged ion with a characteristic dimension much smaller than the Debye length of the electrolyte. On the right is a charged microsphere with a diameter much larger than the Debye length.

where q is the total molecule charge and d is the particle's Stokes diameter (the diameter of a sphere of equal drag). In comparison, the electrophoresis of relatively large solid particles such as 100–10,000 nm diameter polystyrene spheres, clay particles, and single-celled organisms is a function of the electrostatic forces on the surface charge, the electrostatic forces on their charge double layers, and the viscous drag associated with both the motion of the body as well as the motion of the ionic cloud. For a wide range of cases where the particle-diameter–to–Debye-length ratio is large so that locally the ionic cloud near the particle surface can be approximated by the EDL relations for a flat plate, the velocity of an electrophoretic particle reduces simply to

$$u = \frac{\varepsilon \zeta E}{\mu}(d \gg \lambda_d) \qquad (10.49)$$

where the dimension d in the inequality condition is a characteristic dimension of the particle (e.g., its Stokes diameter). This equation was shown by Smoluchowski (1903) to be independent of particle shape. This is the Helmholtz-Smoluchowski equation introduced earlier (with a change of sign).

The two expressions above describing the electrophoresis of particles can be expressed in terms of a mobility v_{eph} equal to $q/(3\pi\mu d)$ and $\varepsilon\zeta/\mu$ for characteristic particle dimensions much smaller and much larger than the Debye length, respectively. Note also that for the simple case of a fluid with uniform properties, the solution of the drift velocity of electrophoretic particles with respect to the bulk liquid are similar (i.e., parallel and directly proportional) to lines of electric field.

Several solutions of the particle velocity and velocity field in the region of an electrophoretic particle with a finite EDL exist [Hunter, 1981; Russel et al., 1999]. A well-known solution is that of Henry (1948) for the flow around an electrophoretic sphere in the Debye-Huckle limit. The $d \gg \lambda_d$ limit of Henry's solution results in Equation (10.49).

10.2.5 Similarity Between Electric and Velocity Fields for Electroosmosis and Electrophoresis

The previous sections have described the solution for electroosmotic velocity field in straight, uniform cross-section channels. In general, solving for the electroosmotic velocity field in more complex geometries requires a solution of the electric field and charge density in the microchannel, together with a solution to the Navier-Stokes equations. A simplification of this flow problem first proposed by Overbeek (1952) suggests that the electroosmotic velocity is everywhere parallel to the electric field for simple electroosmotic flows at low Reynolds numbers. This concept is also discussed by Cummings et al. (2000) and Santiago (2001). Santiago (2001) describes a set of sufficient conditions for which there exist a velocity field solution that is similar to the electric field:

- Uniform zeta potential
- Electric double-layers thin compared to channel dimension
- Electrically insulating channel walls
- Low Reynolds number
- Low product of Reynolds and Strouhal numbers
- Parallel flow at inlets and outlets
- Uniform electrolyte properties (including temperature)

When these conditions are met, the electroosmotic streamlines exactly correspond to the electric field lines. The approximation is applicable to systems with a microchannel length scale less than 100 μm, a AQ16
Debye length less than 10 nm, a velocity scale less than 1 mm/sec, and a characteristic forcing function time scale greater than 10 msec [Santiago, 2001]. An important part of this similarity proof is to show the applicability of the Helmholtz-Smoulochowski equation in describing the local velocity field at the slip surface that bounds the internal flow of the microchannel that excludes the EDL. The Helmholtz-Smoulochowski equation can be shown to hold for most microfluidic systems where the motion of the EDL is dominated by the Lorentz and viscous forces. In such systems, we can consider the velocity field

of the fluid outside of the EDL as a three-dimensional, unsteady flow of a viscous fluid of zero net charge that is bounded by the following slip velocity condition:

$$u_{\text{slip}} = \frac{-\varepsilon\zeta}{\mu} E_{\text{slip}} \tag{10.50}$$

where the subscript *slip* indicates a quantity evaluated at the slip surface at the top of the EDL (in practice, a few Debye lengths from the wall). The velocity along this slip surface is, for thin EDLs, similar to the electric field. This equation and the condition of similarity also hold for inlets and outlets of the flow domain that have zero imposed pressure-gradients.

    The complete velocity field of the flow bounded by the slip surface (and inlets and outlets) can be shown to be similar to the electric field [Santiago, 2001]. We nondimensionalize the Navier–Stokes equations by a characteristic velocity and length scale U_s and L_s respectively. The pressure p is nondimensionalized by the viscous pressure $\mu U_s/L_s$. The Reynolds and Strouhal numbers are $\text{Re} = \rho L_s U_s/\mu$ and $\text{St} = L_s/\tau U_s$, respectively, where τ is the characteristic time scale of a forcing function. The equation of motion is

$$\text{ReSt}\,\frac{\partial \mathbf{u}'}{\partial t'} + \text{Re}(\mathbf{u}' \cdot \nabla \mathbf{u}') = -\nabla p' + \nabla^2 \mathbf{u}' \tag{10.51}$$

Note that the right-most term in Equation (10.51) can be expanded using a well-known vector identity

$$\nabla^2 \mathbf{u}' = \nabla(\nabla \cdot \mathbf{u}') - \nabla \times \nabla \times \mathbf{u}'. \tag{10.52}$$

We can now propose a solution to Equation (10.52) that is proportional to the electric field and of the form

$$\mathbf{u}' = \frac{c_o}{U_s}\mathbf{E} \tag{10.53}$$

where c_o is a proportionality constant, and $\mathbf{E}$ is the electric field driving the fluid. Since we have assumed that the EDL is thin, the electric field at the slip surface can be approximated by the electric field at the wall. The electric field bounded by the slip surface satisfies Faraday's and Gauss' laws,

$$\nabla \cdot \mathbf{E} = \nabla \times \mathbf{E} = 0 \tag{10.54}$$

Substituting Equation (10.53) and Equation (10.54) into Equation (10.51) yields

$$\text{ReSt}\,\frac{\partial \mathbf{u}'}{\partial t'} + \text{Re}(\mathbf{u}' \cdot \nabla \mathbf{u}') = -\nabla p' \tag{10.55}$$

This is the condition that must hold for Equation (10.53) to be a solution to Equation (10.51). One limiting case where this holds is for very high Reynolds number flows where inertial and pressure forces are much larger than viscous forces. Such flows are found in, for example, high speed aerodynamics regimes and are not applicable to microfluidics. Another limiting case applicable here is when Re and ReSt are both small, so that the condition for Equation (10.53) to hold becomes

$$\nabla p' = 0. \tag{10.56}$$

    Therefore we see that for small Re and ReSt and the pressure gradient at the inlets and outlets equal to zero, Equation (10.53) is a valid solution to the flow bounded by the slip surface, inlets, and outlets (note that these arguments do not show the uniqueness of this solution). We can now consider the boundary conditions required to determine the value of the proportionality constant c_o. Setting Equation (10.50) equal to Equation (10.53) we see that $c_o = \varepsilon\zeta/\eta$. So that, if the simple flow conditions are met, then the velocity everywhere in the fluid bounded by the slip surface is given by Equation (10.57).

$$\mathbf{u}(x, y, z, t) = -\frac{\varepsilon\zeta}{\mu}\,\mathbf{E}(x, y, z, t) \tag{10.57}$$
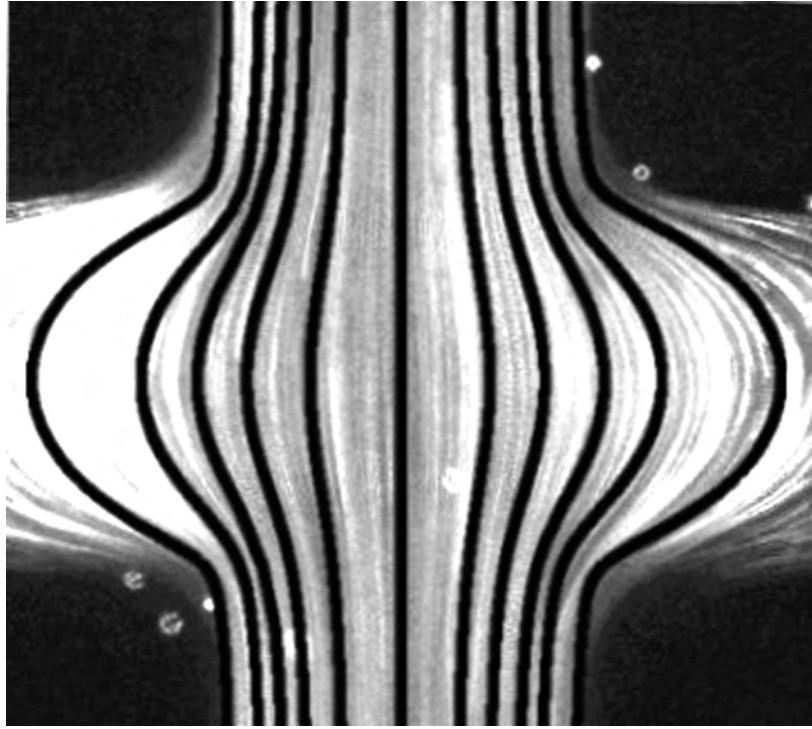
FIGURE 10.13   Comparison between experimentally determined electrokinetic particle pathlines at a microchannel intersection and predicted electric field lines. The light streaks show the path lines of 0.5 μm diameter particles advecting through an intersection of two microchannels. The electrophoretic drift velocities and electroosmotic flow velocities of the particles are approximately equal. The channels have a trapezoidal cross-section having a hydraulic diameter of 18 μm (130 μm wide at the top, 60 μm wide at the base, and 50 μm deep). The superposed heavy black lines correspond to a prediction of electric field lines in the same geometry. The predicted electric field lines very closely approximate the experimentally determined pathlines of the flow. (Reprinted with permission from Devasenathipathy, S. and Santiago, J.G. [2000] unpublished results, Stanford University.)

Equation (10.57) is the Helmholtz-Smoluchowski equation shown to be a valid solution to the quasi-steady velocity field in electroosmotic flow with ζ the value of the zeta potential at the slip surface. This result greatly simplifies the modeling of simple electroosmotic flows since simple Laplace equation solvers can be used to solve for the electric potential and then using Equation (10.57) for the velocity field. This approach has been applied to the optimization of microchannel geometries and verified experimentally [Bharadwaj et al., 2002; Devasenathipathy et al., 2002; Mohammadi et al., 2003; Molho et al., 2001; Santiago, 2001]. An increasing number of researchers have recently applied this result in analyzing electrokinetic microflows [Bharadwaj et al., 2002; Cummings and Singh, 2003; Devasenathipathy et al., 2002; Dutta et al., 2002; Fiechtner and Cummings, 2003; Griffiths and Nilson, 2001; MacInnes et al., 2003; Santiago, 2001]. Figure 10.13 shows the superposition of particle pathlines/streamlines and predicted electric field lines [Santiago, 2001] in a steady flow that meets the simple electroosmotic flow conditions summarized above. As shown in the figure, the electroosmotic flow field streamlines are very well approximated by electric field lines.

For the simple electroosmotic flow conditions analyzed here, the electrophoretic drift velocities (with respect to the bulk fluid) are also similar to the electric field, as mentioned above. Therefore, the time-averaged, total (local drift plus local liquid) velocity field of electrophoretic particles can be shown to be

$$\mathbf{u}_{\text{particle}} = \left(v_{\text{eph}} - \frac{\varepsilon\zeta}{\mu}\right)\mathbf{E}. \tag{10.58}$$

Here, we use the electrophoretic mobility ν_{eph} that was defined earlier, and $\varepsilon\zeta/\mu$ is the electroosmotic flow mobility of the microchannel walls. These two flow field components have been measured by Devasenathipathy et al. (2002) in two- and three-dimensional electrokinetic flows.

10.2.6 Electrokinetic Microchips

The advent of microfabrication and microelectromechanical systems (MEMS) technology has seen an application of electrokinetics as a method for pumping fluids on microchips [Auroux et al., 2002; Bruin, 2000; Jacobson et al., 1994; Manz et al., 1994; Reyes et al., 2002; Stone et al., 2004]. On-chip electroosmotic pumping is easily incorporated into electrophoretic and chromatographic separations, and laboratories on a chip offer distinct advantages over the traditional, freestanding capillary systems. Advantages include reduced reagent use, tight control of geometry, the ability to network and control multiple channels on chip, the possibility of massively parallel analytical process on a single chip, the use of chip substrate as a heat sink (for high field separations), and the many advantages that follow the realization of a portable device [Khaledi, 1998; Stone et al. 2004]. Electrokinetic effects significantly extend the current design space of microsystems technology by offering unique methods of sample handling, mixing, separation, and detection of biological species including cells, microparticles, and molecules.

This section presents typical characteristics of an electrokinetic channel network fabricated using microlithographic techniques (see description of fabrication in the next section). Figure 10.14 shows a top view schematic of a typical microchannel fluidic chip used for capillary electrophoresis [Bruin, 2000; Manz et al., 1994; Stone et al., 2004]. In this simple example, the channels are etched on a dielectric substrate and bonded to a clear plate of the same material (e.g., coverslip). The circles in the schematic represent liquid reservoirs that connect with the channels through holes drilled through the coverslip. The parameters V_1 through V_4 are time-dependent voltages applied at each reservoir well. A typical voltage switching system may apply voltages with on/off ramp profiles of approximately 10,000 V/s or less so that the flow can often be approximated as quasi-steady.

The four-well system shown in Figure 10.14 can be used to perform an electrophoretic separation by injecting a sample from well #3 to well #2 by applying a potential difference between these wells. During this injection phase, the sample is confined, or pinched, to a small region within the separation channel by flowing solution from well #1 to #2 and from well #4 to well #2. The amount of desirable pinching is generally a tradeoff between separation efficiency and sensitivity. Ermakov et al. (2000), Alarie et al. (2000), and Bharadwaj et al. (2002) all present optimizations of the electrokinetic sample injection process. Next, the injection phase potential is deactivated and a potential is applied between well 1 and well #4 to dispense the injection plug into the separation channel and begin the electrophoretic separation. The potential between wells #1 and #2 is referred to as the separation potential. During the separation phase, potentials are applied at wells #2 and #3, which "retract," or "pull back," the solution-filled streams on either side of the separation channel. As with the pinching described above, the amount of "pull back" is a trade-off between separation efficiency and sensitivity. As discussed by Bharadwaj et al.
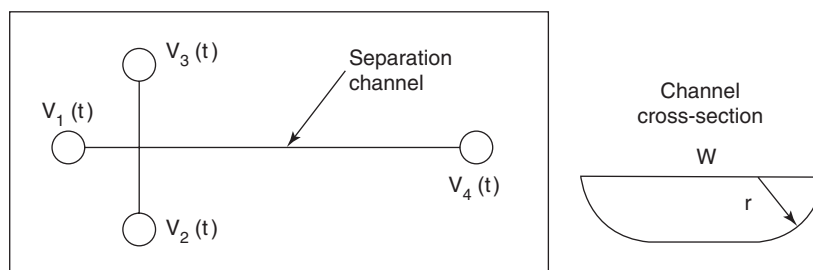

FIGURE 10.14   Schematic of a typical electrokinetic microchannel chip. V_1 through V_5 represent time-dependent voltages applied to each microchannel. The channel cross-section shown is for the (common case) of an isotropically etched glass substrate with a mask line width of $(w - 2r)$.

(2002), additional injection steps (such as a reversal of flow from well #2 to #1)for a short period prior to injection and pull back) can minimize the dispersion of sample during injection.

Figure 10.15 shows a schematic of a system that was used to perform and image an electrophoretic separation in a microfluidic chip. The microchip depicted schematically in Figure 10.15 is commercially available from Micralyne, Inc., Alberta, Canada. The width and depth of the channels are 50 μm and 20 μm respectively. The separation channel is 80 mm from the intersection to the waste well (well #4 in Figure 10.14). A high voltage switching system allows for rapid switching between the injection and separation voltages and a computer, epifluorescent microscope, and CCD camera are used to image the electrophoretic separation. The system depicted in Figure 10.15 is used to design and characterize electrokinetic injections; in a typical electrophoresis application, the CCD camera would be replaced with a point detector (e.g., a photo-multiplier tube) near well #4.

Figure 10.16 shows an injection and separation sequence of 200 μM solutions of fluorescein and Bodipy dyes (Molecular Probes, Inc., Eugene, Oregon). Images 10.16a through 10.16d are each 20 msec exposures separated by 250 msec. In Figure 16a, the sample is injected applying 0.5 kV and ground to well #3 and well #2, respectively. The sample volume at the intersection is pinched by flowing buffer from well #1 and well #4. Once a steady flow condition is achieved, the voltages are switched to inject a small sample plug into the separation channel. During this separation phase, the voltages applied at well #1 and well #4 are 2.4 kV and ground respectively. The sample remaining in the injection channel is retracted from the intersection by applying 1.4 kV to both well #2 and well #3. During the separation, the electric field strength in the separation channel is about 200 V/cm. The electrokinetic injection introduces an approxi- [AQ18] mately 400 pl volume of the homogeneous sample mixture into the separation channel, as seen in Figure 10.16b. The Bodipy dye is neutral, and therefore its species velocity is identical to that of the electroosmotic flow velocity. The relatively high electroosmotic flow velocity in the capillary carries both the neutral Bodipy and negatively charged fluorescein toward well #4. The fluorescein's negative electrophoretic mobility moves it against the electroosmotic bulk flow, and therefore it travels more slowly than the Bodipy dye. This difference in electrophoretic mobilities results in a separation of the two dyes into distinct analyte bands, as seen in Figures 10.16c and 10.16d. The zeta potential of the microchannel walls for the system used in this experiment was estimated at −50 mV from the velocity of the neutral Bodipy dye [Bharadwaj and Santiago, 2002]. The inherent trade-offs between initial sample plug length, electric field,
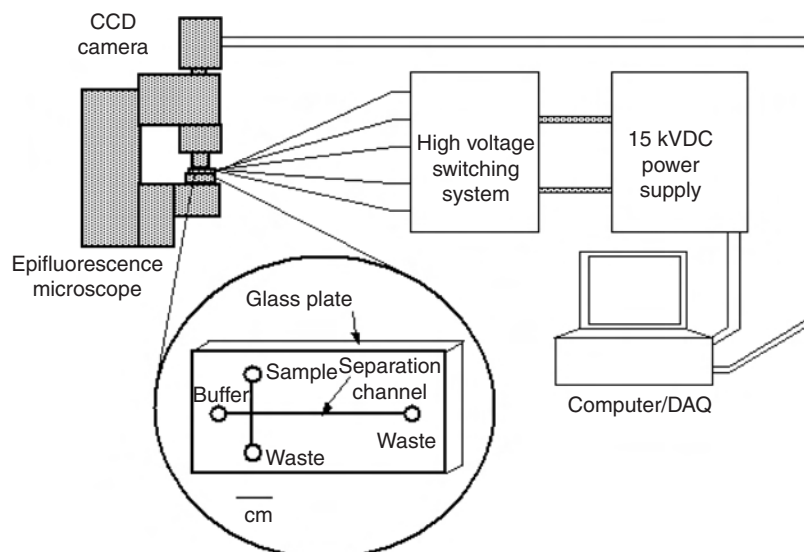

FIGURE 10.15   Schematic of microfabricated capillary electrophoresis system, flow imaging system, high voltage control box, and data acquisition computer.
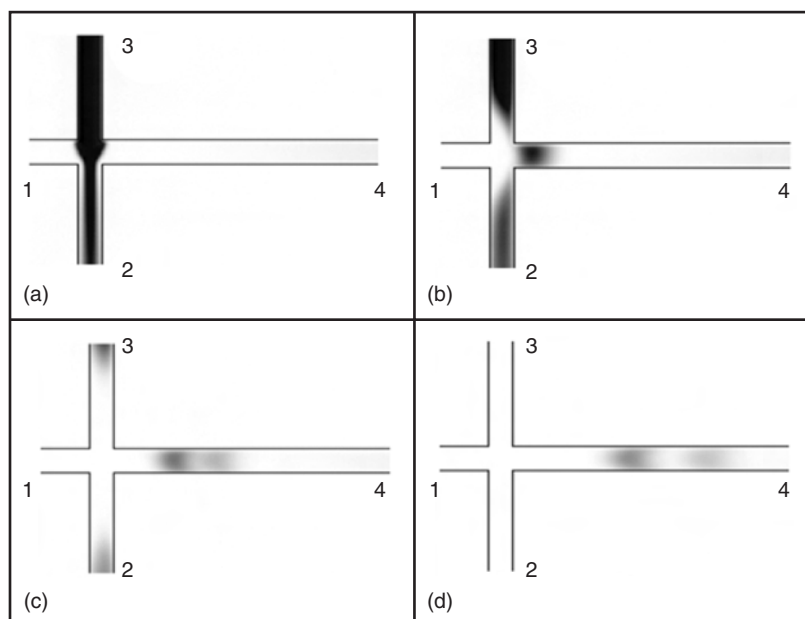
FIGURE 10.16   Separation sequence of Bodipy and fluorescein in a microfabricated capillary electrophoresis system. The channels shown are 50 μm wide and 20 μm deep. The fluoresceine images are 20 msec exposures and consecutive images are separated by 250 msec. A background image has been subtracted from each of the images, and the channel walls were drawn in for clarity. (Reprinted with permission from Bharadwaj, R. and Santiago, J.G. [2000] unpublished results, Stanford University.)

channel geometry, separation channel length, and detector characteristics are discussed in detail by Bharadwaj et al. (2002). Kirby and Hasselbrink (2004) present a review of electrokinetic flow theory and methods of quantifying zeta potentials in microfluidic systems. Ghosal (2004) presents a review of band-broadening effects in microfluidic electrophoresis.

10.2.7 Engineering Considerations: Flow Rate and Pressure of Simple Electroosmotic Flows

As we have seen, the velocity field of simple electrokinetic flow systems with thin EDLs is approximately independent of the location in the microchannel and is therefore a "plug flow" profile for any cross-section of the channel. The volume flow rate of such a flow is well approximated by the product of the electroosmotic flow velocity and the cross-sectional area of the inner capillary:

$$Q = -\frac{\varepsilon\zeta EA}{\mu}. \tag{10.59}$$

For the typical case of electrokinetic systems with a bulk ion concentration in excess of about 100 μM and characteristic dimension greater than about 10 μm, the vast majority of the current carried within the microchannel is the electromigration current of the bulk liquid. For such typical flows, we can rewrite the fluid flow rate in terms of the net conductivity of the solution, σ,

$$Q = -\frac{\varepsilon\zeta I}{\mu\sigma}, \tag{10.60}$$

where I is the current consumed, and we have made the reasonable assumption that the electromigration component of the current flux dominates. The flow rate of a microchannel is therefore a function of the current carried by the channel and otherwise independent of geometry.
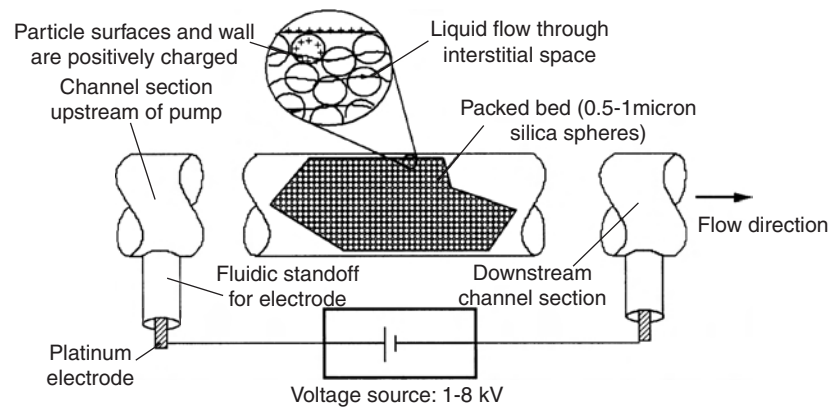
FIGURE 10.17   Schematic of electrokinetic pump fabricated using a glass microchannel packed with silica spheres. The interstitial spaces of the packed bead structure create a network of submicron microchannels that can be used to generate pressures in excess of 5000 psi.

Another interesting case is that of an electrokinetic capillary with an imposed axial pressure gradient. For this case, we can use Equation (10.47) to show the magnitude of the pressure that an electrokinetic microchannel can achieve. To this end, we solve Equation (10.47) for the maximum pressure generated by a capillary with a sealed end and an applied voltage ΔV, noting that the electric field and the pressure gradient can be expressed as $\Delta V/L$ and $\Delta p/L$ respectively. Such a microchannel will produce zero net flow but will provide a significant pressure gradient in the direction of the electric field (in the case of a negatively charged wall). Imposing a zero net flow condition $Q = \int_A \mathbf{u} \cdot dA = 0$ the solution for pressure generated in a thin EDL microchannel is then

$$\Delta p = -\frac{8\varepsilon\zeta\Delta V}{a^2} \tag{10.61}$$

which shows that the generated pressure will be directly proportional to voltage and inversely proportional to the square of the capillary radius. Equation (10.61) dictates that decreasing the characteristic radius of the microchannel will result in higher pressure generation. The following section discusses a class of devices designed to generate both significant pressures and flow rate using electroosmosis.

10.2.8   Electroosmotic Pumps

EO pumps are devices that generate both significant pressure and flow rate using electroosmosis through pores or channels. A review of the history and technological development of such electroosmotic pumps is presented by Yao and Santiago (2003a). The first electroosmotic pump structure (generating significant pressure) was demonstrated by Theeuwes in 1975. Other notable contributions include that of Gan et al. (2000), who demonstrated pumping of several electrolyte chemistries; and Paul et al. (1998a) and Zeng et al. (2000), who demonstrated of order 10 atm and higher. Yao et al. (2003b) presented experimentally validated, full Poisson-Boltzmann models for porous electroosmotic pumps. They demonstrated a pumping structure less than $2\,cm^3$ in volume that generates 33 ml/min and 1.3 atm at 100 V.

Figure 10.17 shows a schematic of a packed-particle bed electroosmotic pump of the type discussed by Paul et al. (1998a) and Zeng et al. (2000). This structure achieves a network of submicron diameter microchannels by packing 0.5–1 micron spheres in fused silica capillaries, using the interstitial spaces in these packed beds as flow passages. Platinum electrodes on either end of the structure provide applied potentials on the order of 100 to 10,000 V. A general review of micropumps that includes sections on electroosmotic pumps is given by Laser and Santiago (2004).

10.2.9   Electrical Analogy and Microfluidic Networks

There is a strong analogy between electroosmotic and electrophoretic transport and resistive electrical networks of microchannels with long axial-to-radial dimension ratios. As described above, the electroosmotic flow rate is directly proportional to the current. This analogy holds provided that the previously described conditions for electric/velocity field similarity also hold. Therefore, Kirkoff's current and voltage laws can be used to predict flow rates in a network of electroosmotic channels given voltage at endpoint nodes of the system. In this one-dimensional analogy, all of the current, and hence all of the flow, entering a node must also leave that node. The resistance of each segment of the network can be determined by knowing the cross-sectional area, the conductivity of the liquid buffer, and the length of the segment. Once the resistances and applied voltages are known, the current and electroosmotic flow rate in every part of the network can be determined using Equation (10.60).

10.2.10   Electrokinetic Systems with Heterogenous Electrolytes

The previous sections have dealt with systems with uniform properties such as ion-concentrations (including pH), conductivity, and permittivity. However, many practical electrokinetic systems involve heterogeneous electrolyte systems. A general transport model for heterogenous electrolyte systems (and indeed for general electrohydrodynamics) should include formulations for the conservation of species, Gauss' law, and the Navier-Stokes equations describing fluid motion [Castellanos, 1998; Melcher, 1981; Saville, 1997]. The solutions to these equations can in general be a complex nonlinear coupling of these equations. Such a situation arises in a wide variety of electrokinetic flow systems. This section presents a few examples of recent and ongoing work in these complex electrokinetic flows.

10.2.10.1   Field Amplified Sample Stacking (FASS)

Sensitivity to low analyte concentrations is a major challenge in the development of robust bioanalytical devices. Field amplified sample stacking (FASS) is one robust way to carry out on-chip sample preconcentration. In FASS, the sample is prepared in an electrolyte solution of lower concentration than the background electrolyte (BGE). The low-conductivity sample is introduced into a separation channel otherwise filled with the BGE. In these systems, the electromigration current is approximately nondivergent so that $\nabla \cdot (\sigma \overline{E}) = 0$, where σ is ionic conductivity. Upon application of a potential gradient along the axis of the separation channel, the sample region is therefore a region of low conductivity (high electric field) in series with the BGE region(s) of high conductivity (low electric field). Sample ions migrate from the high-field–high-drift-velocity of the sample region to the low-field–low-drift-velocity region and accumulate, or stack, at the interface between the low and high conductivity regions.

   The seminal work in the analysis of unsteady ion distributions during electrophoresis is that of Mikkers et al. (1979), who used the Kohlrausch regulating function (KRF) [Beckers and Bocek, 2000; Kohlrausch, 1897] to study concentration distributions in electrophoresis. There have been several review papers on FASS, including discussions of on-chip FASS devices, by Quirino et al. (1999), Osborn et al. (2000), and Chien (2003). FASS has been applied by Burgi and Chien (1991), Yang and Chien (2001), and Lichtenberg et al. (2001) to microchip-based electrokinetic systems. These three studies demonstrated maximum signal enhancements of 100-fold over nonstacked assays. More recently, Jung et al. (2003) demonstrated a device that avoids electrokinetic instabilities associated with conductivity gradients and achieves a 1,100-fold increase in signal using on-chip FASS. Recent modeling efforts include the work of Sounart and Baygents (2001), who developed a multicomponent model for electroosmotically driven separation processes. They performed two-dimensional numerical simulations and demonstrated that nonuniform electroosmosis in these systems causes regions of recirculating flow in the frame of the moving analyte plug. These recirculating flows can drastically reduce the efficiency of sample stacking. Bharadwaj and Santiago (2004) present an experimental and theoretical investigation of FASS dynamics. Their model analyzes dispersion dynamics using a hybrid analysis method that combines area-averaged, convective-diffusion equations with regular perturbation methods to provide a simplified equation set

for FASS. They also present model validation data in the form of full-field epifluorescence images quantifying the spatial and temporal dynamics of concentration fields in FASS.

The dispersion dynamics of nonuniform electroosmotic flow FASS systems results in concentration enhancements that are a strong function of parameters such as electric field, electroosmotic mobility, diffusivity, and the background electrolyte-to-sample conductivity ratio γ. At low γ and low electroosmotic mobility, electrophoretic fluxes dominate transport and concentration enhancement increases with γ. At γ and significant electroosmotic mobilities, increases in γ increase dispersion fluxes and lower sample concentration rates. The optimization of this process is discussed in detail by Bharadwaj and Santiago (2004).

AQ19 10.2.10.2 Isothachopheresis

Isothachopheresis (Everaerts et al., 1976) uses a heterogenous buffer to achieve both concentration and separation of charged ions or macromolecules. Isotachophoresis (ITP) occurs when a sample plug containing anions (or cations) is sandwiched between a trailing buffer and a leading buffer such that all the sample anions (cations) are slower than the anion (cation) in the leading buffer and faster than all the anion (cation) in the trailing buffer. When an electric field is applied in this situation, all the sample anions (cations) will rapidly form distinct zones that are arranged by electrophoretic mobility. In the case where each sample ion carries the bulk of the current in its respective zone, the KRF states that the final concentration of each ion will be proportional to its mobility. Because all anions (cations) migrate in distinct zones, current continuity ensures that they migrate at the same velocity (hence the name *isotacho*phoresis), resulting in characteristic translating conductivity boundaries. Isotachophoresis in a transient manner is used as a preconcentration technique prior to capillary electrophoresis; this combination is often referred to as ITP-CE (Hirokawa 2003). Isotachophoresis and ITP-CE in microdevices has been described by Kaniansky et al. (2000), Vreeland et al. (2003), Wainright et al. (2002), and Xu et al. (2003).

10.2.10.3 Isoelectric focusing

Isoelectric focusing (IEF) is another electrophoretic technique that utilizes heterogenous buffers to achieve concentration and separation [Catsimpoolas 1976; Righetti, 1983]. Isoelectric focusing usually employs a background buffer containing carrier ampholytes (molecules that can be either negatively charged, neutral, or positively charged depending on the local pH). The pH at which an amphoteric molecule is neutral is called the isoelectric point, or pI. Under an applied electric field, the carrier ampholytes create a pH gradient along a channel or capillary. When other amphoteric sample molecules are introduced into a channel with such a stabilized pH gradient, the samples migrate until they reach the location where the pH is equal to the pI of the sample molecule. Thus IEF concentrates initially dilute amphoteric samples and separate them by isoelectric point. Because of this behavior, IEF is often used as the first dimension of multidimensional separations. IEF and multidimensional separations employing IEF have been demonstrated in microdevices by Hofmann et al. (1999), Woei et al. (2002), Li et al. (2004), Macounova et al. (2001), and Herr et al. (2003).

10.2.10.4 Temperature Gradient Focusing

Another method of sample stacking is temperature gradient focusing (TGF), which uses electrophoresis, pressure-driven flow, and electroosmosis to focus and separate samples based on electrophoretic mobility. In TGF, an axial temperature gradient applied axially along a microchannel produces a gradient in electrophoretic velocity. When opposed by a net bulk flow, charged analytes focus at points where their electrophoretic velocity and the local, area-averaged liquid velocity sum to zero. The method has been demonstrated experimentally by Ross and Locascio (2002). A review of various various electrofocusing techniques is given by Ivory (2000).

10.2.10.5 Electrothermal Flows

A fifth important class of heterogenous electrolyte electrokinetic flows are electrothermal flows. These flows are generated by electric body forces in the bulk liquid of an electrokinetic flow system with finite temperature

gradients. These flows were first described by Ramos et al. (1998) and have been analyzed by Ramos et al. (1999) and Green et al. (2000a, 2000b). Work in this area is summarized in the book by Morgan and Green (2003). These researchers were interested in steady flow-streaming-like behavior observed in microfluidic systems with patterned AC electrodes. The devices were designed for dielectrophoretic particle concentration and separation. Secondary flows in these systems are generated by the coupling of AC electric fields and temperature gradients. This coupling creates body forces that can cause order 100 micron per second liquid velocities and dominate the transport of particulates in the device. Experimental validation of these flows has been presented by Green et al. (2000b) and Wang et al. (2004). The latter work used two-color micron-resolution PIV (Santiago, 1998) to independently quantify liquid and particle velocity fields.

Ramos et al. (1998) presented a linearized theory for modeling electrothermal flows. Electrothermal forces result from net charge regions in the bulk of an electrolyte with finite temperature gradients. Temperature gradients are a result of localized Joule heating in the system and affect both local electrical conductivity σ and the dielectric permittivity ε. In the Ramos model, ion density is assumed uniform and the temperature field (and therefore the conductivity and permittivity fields) is assumed known and steady. The latter assumptions imply a low value of the thermal Peclet number (Probstein, 1994) for the flow. The general body force on a volume of liquid in this system, $\bar{f}_e$ can be derived from the divergence of the Maxwell stress tensor (Melcher, 1981) and written as

$$\bar{f}_e = \rho_E \bar{E} - 0.5|\bar{E}|^2 \nabla\varepsilon$$

Ramos et al. (1998) assume a linear expansion of the form $\bar{E} = \bar{E}_o + \bar{E}_1$, where $\bar{E}_o$ is the applied field (satisfying $\nabla \cdot \bar{E}_o = 0$) and $\bar{E}_1$ is the perturbed field, such that $|E_o| \gg |E_1|$. Assuming a sinusoidal applied field of the form $\bar{E}_o(t) = \text{Re}[\bar{E}_o \exp(j\omega t)]$, and substituting this linearization into an expression of the conservation of electromigration current ($\nabla \cdot (\sigma\bar{E}) = 0$), yields

$$\nabla \cdot \bar{E}_1 = \frac{-(\nabla\sigma + j\omega\nabla\varepsilon) \cdot \bar{E}_o}{\sigma + j\omega\varepsilon},$$

where higher order terms have been neglected. The (steady, nonuniform) electric charge density is then $\rho_E = \nabla\varepsilon \cdot \bar{E}_o + \varepsilon\nabla \cdot \bar{E}_1$. This charge density can be combined with the relation for $\bar{f}_e$ above to solve for motion of the liquid using the Navier–Stokes equations. Note that this model assumes steady conductivity and permittivity fields determined solely by a steady temperature field. The electric body force field is therefore uncoupled from the motion of the liquid.

10.2.10.6 Electrokinetic Flow Instabilities

Electrokinetic instabilities are a sixth interesting example of complex electrokinetic flow in heterogenous electrolyte systems. Electrokinetic instabilities (EKI) are produced by an unsteady coupling between electric fields and conductivity gradients. Lin et al. (2004) and Chen et al. (2004) present the derivation of a model for generalized electrokinetic flow that builds on the general electrohydrodynamics framework provided by Melcher (1981). This model results in a formulation of the following form:

$$\frac{\partial\sigma}{\partial t} + \mathbf{v} \cdot \nabla\sigma = \frac{1}{Ra_e}\nabla^2\sigma,$$

$$\nabla \cdot (\sigma\bar{E}) = 0,$$

$$\nabla \cdot \varepsilon\bar{E} = \rho_E,$$

$$\nabla \cdot \mathbf{v} = 0,$$

$$\text{Re}\left(\frac{\partial\mathbf{v}}{\partial t} + \mathbf{v} \cdot \nabla\mathbf{v}\right) = -\nabla p + \nabla^2\mathbf{v} + \rho_E\bar{E}.$$

The first equation governs the development of the unsteady, nonuniform electrolyte conductivity, σ, and is derived from a summation of the charged species equations. The second equation is derived from a
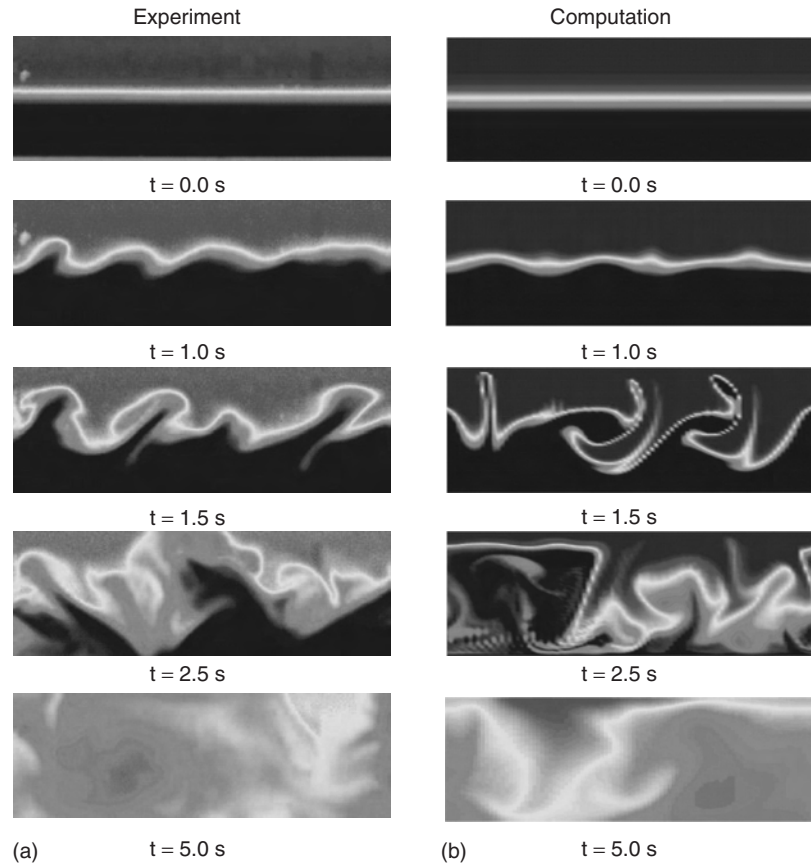
Experiment   Computation

t = 0.0 s   t = 0.0 s

t = 1.0 s   t = 1.0 s

t = 1.5 s   t = 1.5 s

t = 2.5 s   t = 2.5 s

(a)   t = 5.0 s   (b)   t = 5.0 s

FIGURE 10.18 Time evolution of electrokinetic flow instability: (a) Experimental data of instability mixing of HEPES buffered 50 μS/cm (red) and 5 μS/cm (blue) conductivity streams [Lin et al., 2004]. At time t = 0.0 sec, a static electric field of E = 50,000 V/m is applied in the (horizontal) streamwise direction perpendicular to the initial conductivity gradients. Image area is 1 mm in the vertical direction and 3.6 mm in the streamwise direction. Channel depth (into the page) is 100 μm. Small amplitude waves quickly grow and lead to rapid stirring of the initially distinct buffer streams. (b) Reproduction of dynamics from simplified, 2-D nonlinear numerical computations. The numerical model well reproduces features of the instability observed in experiments, including wave number and time scale. Details of this model are given by Lin et al. [2004].

conservation of net charge in the limit of fast charge relaxation. As discussed in detail by Lin et al. (2004), the relaxed charge assumption is consistent with the net neutrality approximation and leads to the condition that electromigration current is at all times conserved. The third equation is Gauss' law, and the last two are the Navier–Stokes equations describing fluid velocity with an electrostatic body force of the form $\rho_E \bar{E}$. Electrokinetic flow instabilities associated with electrokinetic flows with conductivity gradients arise from a coupling of these equations. This coupling results in an electric body force (per unit volume) of the form $(\varepsilon \bar{E} \cdot \nabla \sigma)\bar{E}$, which occurs in regions where local electric field is parallel to the conductivity gradient. Electrokinetic flows become unstable when the ratio of the characteristic electric body force to the viscous force in the flow exceeds a critical value [Chen et al., 2004; Lin et al., 2004]. These flows are unstable even in the limit of vanishing Reynolds number.

Electrokinetic instabilities have been experimentally demonstrated, for various geometric configurations by Oddy et al. (2001), Lin et al. (2004), and Chen et al. (2002, 2004). Figure 10.18 shows both an experimental visualization and a numerical model of a temporal instability in a microchannel with a conductivity gradient initially orthogonal to the applied electric field [Oddy, 2001]. Chen et al. (2004) show,

in a slightly different geometry with much shallower channel (11 micron depth), a convective electrokinetic instability in which spatial growth of disturbances is observed. In both of these experiments threshold electric fields are observed above which the flow becomes unstable and rapid stirring and mixing occur. Together, the work of Lin et al. (2004) and Chen et al. (2004) describes the basic mechanism behind electrokinetic instabilities and identifies the critical electric Rayleigh numbers that govern the onset of the instability. Lin et al. (2004) present linear models for temporal electrokinetic instabilities, a nonlinear numerical model of the instability, and validation experiments in a long, thin microchannel structure. Chen et al. (2004) also present experimental results and describe the convective nature of the instability. The latter work identifies the electroviscous–to–electroosmotic-velocity ratio as the critical value that demarcates the boundary between convective and absolute instability.

In general, electrokinetic instabilities and flows with unsteady, nonuniform body forces due to couplings between electric fields and conductivity and permittivity gradients are directly relevant to a variety of on-chip electrokinetic systems. Such complex flow systems include field amplified sample stacking devices [Bharadwaj and Santiago, 2004; Chien, 2003; Jung et al., 2003]; low-Reynolds number micromixing [Oddy et al., 2001]; multidimensional assay systems [Herr et al., 2003]; and dielectrophoretic devices [Morgan and Green, 2003]. In general, this complex coupling of applied field and heterogenous electrolyte properties may occur in any electrokinetic system with imperfectly specified sample chemistry.

10.2.11   Practical Considerations

A few practical considerations should be considered in the design, fabrication, and operation of electrokinetic microfluidic systems. These considerations include the dimensions of the system, the choice of liquid and buffer ions, the field strengths used, and the characteristics of the flow reservoirs and interconnects. A few examples of these design issues are given here.

In the case of microchannels used to generate pressure, Equation (10.60) shows that a low liquid conductivity is essential for increasing thermodynamic efficiency of an electrokinetic pump because Joule heating is an important contributor to dissipation [Yao and Santiago, 2003a; Zhao and Liao, 2002]. In electrokinetic systems for chemical analysis, on the other hand, the need for a stable pH requires a finite buffer strength, and typical buffer strengths are in the 1–100 mM range. The need for a stable pH therefore often conflicts with a need for high fields [Bharadwaj et al., 2002] to achieve high efficiency separations because of the effects of Joule heating of the liquid.

Joule heating of the liquid in electrokinetic systems can be detrimental in two ways. First, temperature gradients within the microchannel cause a nonuniformity in the local mobility of electrophoretic particles because the local viscosity is a function of temperature. This nonuniformity in mobility results in a dispersion associated with the transport of electrophoretic species [Bosse and Arce, 2000; Grushka et al., 1989; Knox, 1988]. The second effect of Joule heating is the rise in the absolute temperature of the buffer. This temperature rise results in higher electroosmotic mobilities and higher sample diffusivities. In microchip electrophoretic separations, the effect of increased diffusivity on separation efficiency is somewhat offset by the associated decrease in separation time. In addition, the authors have found that an important limitation to the electric field magnitude in microchannel electrokinetics is that elevated temperatures and the associated decreases in gas solubility of the solution often result in the nucleation of gas bubbles in the channel. This effect of driving gas out of solution typically occurs well before the onset of boiling and can be catastrophic to the electrokinetic system because gas bubbles grow and eventually break the electrical circuit required to drive the flow. This effect can be reduced by outgassing of the solution and is, of course, a strong function of the channel geometry, buffer conductivity, and the thermal properties of the substrate material.

Another important consideration in any microfluidic device is the design and implementation of macro-to-micro fluidic interconnects. Practical implementations of fluidic interconnects span a wide range of complexity. One common practice (though rarely mentioned in publications) is to simply glue (e.g., with epoxy and by hand) trimmed plastic pipette tips or short glass tubes around the outlet port on a fluidic chip to form an end-channel reservoir. Some systems, such as those described by Gray et al.

(1999) for silicon microfluidic chips, incorporate especially microfabricated structures for integrated, low-dead-volume connections. Krulevitch (2002) describes a set of interconnects applicable to silicone rubber fluidic systems. Still other systems use Nanoport interconnect fittings commercially available from Upchurch Scientific. Fluidic interconnects are clearly an area that would benefit from an informed review of the various advantages and disadvantages of common schemes. These factors include ease of assembly, typical fabrication yield, dead volume, ability to deal with electrolytic reaction products, and pressure capacity.

   Lastly, an important consideration in electrokinetic experiments is the inadvertent application and/or generation of pressure gradients in the microchannel. Probably the most common cause of this is a mismatch in the height of the fluid level at the reservoirs. Although there may not be a mismatch of fluid level at the start of an experiment, the flow rates created by electroosmotic flow may eventually create a fluid level mismatch. Also, the fluid level in each reservoir, particularly in reservoirs of 1 mm diameter or less, may be affected by electrolytic gas generation at each electrode. Because electroosmotic flow rate scales as channel diameter squared, whereas pressure-driven flow scales as channel diameter to the fourth power, this effect is greatly reduced by decreasing the characteristic channel diameter. Another common method of reducing this pressure head effect is to increase the length of the channel for a given cross-section. This length increase, of course, implies an increase in operating voltages to achieve the same flow rate. A second source of pressure gradients is a nonuniformity in the surface charge in the channel. An elegant closed-form solution for the flow in a microchannel with arbitrary axial zeta potential distribution is presented by Anderson and Idol (1985). Herr et al. (2000) visualized this effect and offered a simple analytical expression to the pressure-driven flow components associated with zeta potential gradients in fully developed channel flows.

10.3   Summary and Conclusions

In microchannels, the flow of a liquid differs fundamentally from that of a gas, primarily due to the effects of compressibility and potential rarefaction in gases. Significant differences from continuum macroscale theories have been observed. If experiments are performed with sufficient control and care in channels with dimensions of the order of tens of microns or larger, the friction factors measured in the range of accepted laminar flow behavior (i.e., Re < 2000) agree with classical continuum hydrodynamic theory to within small or negligible differences [Sharp and Adrian, 2004], and the transition to turbulence occurs at or near the nominally accepted values for both rectangular and circular microchannels [Liu and Garimella, 2004; Sharp and Adrian, 2004].

   The possibility cannot be ruled out, however, that some physical effects such as roughness or electrical charge effects are causing a deviation from conventional flow results in certain experiments. Observed differences may also be due to imperfections in the flow system of the experiment, and because imperfections may well occur in real engineering systems, it is essential to understand the sources of the observed discrepancies in order to avoid them, control them, or factor them into the designs. Measurement techniques for liquid flows are advancing quickly, both as macroscale methods are adapted to these smaller scales and as novel techniques are being developed. Further insight into phenomena present in the microscale flows, including those due to imperfections in channels or flow systems, is likely to occur rapidly given the evolving nature of the measurement techniques. Complex, nonlinear channels can be used efficiently to design for functionality.

   Electrokinetics is a convenient and easily controlled method of achieving sample handling and separations on a microchip. Because the body force exerted on the liquid is typically limited to a region within a few nanometers from the wall, the resulting profiles, in the absence of imposed pressure-gradients, are often plug-like for channel dimensions greater than about $10\,\mu$m and ion concentrations greater than about $10\,\mu$M. For simple electroosmotic flows with thin EDLs, low Reynolds number, uniform surface charge, and zero imposed pressure gradients, the velocity field of these systems is well approximated by potential flow theory. This significant simplification can, in many cases, be used to predict and optimize the performance of electrokinetic systems. Further, electrokinetics can be used to generate large pressures

($>$20 atm) on a microfabricated device. In principle, the handling, rapid mixing, and separation of solutes in less than 1 pL sample volumes should be possible using electrokinetic systems built with current microfabrication technologies.

AQ20

References

Adamson, A.W. and Gast, A.P. (1997) "Physical Chemistry of Surfaces," 6th ed., John Wiley & Sons, Inc., New York.

Alarie, J.P., Jacobson, S.C., Culbertson, C.T., et al. (2000) "Effects of the Electric Field Distribution on Microchip Valving Performance," *Electrophoresis* 21, pp. 100–6.

Anderson, J.L. and Idol, W.K. (1985) "Electroosmosis through Pores with Nonuniformly Charged Walls," *Chemical Engineering Communications* 38, pp. 93–106.

Arkilic, E.B., Schmidt, M.A., and Breuer, K.S. (1997) "Gaseous Slip Flow in Long Microchannels," *J. MEMS* 6, pp. 167–78.

Arulanandam, S. and Li, D. (2000) "Liquid Transport in Rectangular Microchannels by Electroosmotic Pumping," *Colloids and Surfaces A* 161, pp. 89–102.

Auroux, P. A., Iossifidis, D., Reyes, D. R., and Manz, A. (2002) "Micro Total Analysis Systems: 2. Analytical Standard Operations and Applications," *Analytical Chemistry* 74, pp. 2637–52.

Baker, D.R. (1995) "Capillary Electrophoresis," in *Techniques in Analytical Chemistry Series,* John Wiley & Sons, Inc., New York.

Beckers, J.L. and Bocek, P. (2000) "Sample Stacking in Capillary Zone Electrophoresis: Principles, Advantages, and Limitations," *Electrophoresis* 21, pp. 2747–67.

Berger, M., Castelino, J., Huang, R., Shah, M., and Austin, R.H. (2001) "Design of a Microfabricated Magnetic Cell Separator," *Electrophoresis* 22, pp. 3883–92.

Bharadwaj, R. and Santiago, J.G. (2004) "Dynamics of Field Amplified Sample Stacking," submitted to *J. Fluid Mec*.

Bharadwaj, R., Santiago, J.G., and Mohammadi, B. (2002) "Design and Optimization of On-Chip Electrophoresis," *Electrophoresis* 23, pp. 2729–44.

Bianchi, F., Ferrigno, R., and Girault, H.H. (2000) "Finite Element Simulation of an Electroosmotic-Driven Flow Division at a T-Junction of Microscale Dimensions," *Anal. Chem.* 72, pp. 1987–93.

Blankenstein, G. and Larsen, U.D. (1998) "Modular Concept of a Laboratory on a Chip for Chemical and Biochemical Analysis," *Biosensors & Bioelectronics* 13, pp. 427–38.

Bosse, M.A. and Arce, P. (2000) "Role of Joule Heating in Dispersive Mixing Effects in Electrophoretic Cells: Convective-Diffusive Transport Aspects," *Electrophoresis* 21, pp. 1026–33.

Brandner, J., Fichtner, M., Schygulla, U., and Schubert, K. (2000) "Improving the Efficiency of Micro Heat Exchangers and Reactors," in *Proc. 4th Int'l. Conf. Microreaction Technology*, AIChE, 5–9 March, Atlanta, Georgia, pp. 244–49.

Branebjerg, J., Fabius, B., and Gravesen, P. (1995) "Application of Miniature Analyzers: From Microfluidic Components to TAS," in *Micro Total Analysis Systems*, eds. A. van den Berg and P. Bergveld, Kluwer Academic Publishers, Dordrecht, pp 141–51.

Branebjerg, J., Gravesen, P., Krog, J.P., and Nielsen, C.R. (1996) "Fast Mixing by Lamination," in *Proc. 9th Annual Workshop of Micro Electro Mechanical Systems*, San Diego, California, 11–15 February, pp. 441–46.

Brody, J.P., Yager, P., Goldstein, R.E., and Austin, R.H. (1996) "Biotechnology at Low Reynolds Numbers," *Biophys. J.* 71, pp. 3430–41.

Bruin, G.J.M. (2000) "Recent Developments in Electrokinetically Driven Analysis on Microfabricated Devices," *Electrophoresis* 21, pp. 3931–51.

Brutin, D. and Tadrist, L. (2003) "Experimental Friction Factor of a Liquid Flow in Microtubes," *Phys. Fluids* 15, pp. 653–61.

Burgi, D.S. and Chien, R.L. (1991) "Optimization of Sample Stacking for High Performance Capillary Electrophoresis," *Anal. Chem.* 63, pp. 2042–47.

AQ21

Burgreen, D. and Nakache, F.R. (1964) "ElectroKinetic Flow in Ultrafine Capillary Slits," *J. Phys. Chem.* 68, pp. 1084–91.

Castellanos, A. (1998) *Electrohydrodynamics*, New York, Springer-Verlag Wien.

Catsimpoolas, N. (1976) *Isoelectric Focusing*, New York, Academic Press.

Celata, G.P., Cumo, M., Guglielmi, M., and Zummo, G. (2002) "Experimental Investigation of Hydraulic and Single-Phase Heat Transfer in a 0.130-mm Capillary Tube," *Microscale Thermophys. Eng.* 6, p. 85–97.

Chen, C.-H., Lin, H., Santiago, J.G., and Lele, S. (2004) "Analysis of Convective Electrokinetic Flow Instabilities," submitted to the *J. Fluid Mech*.

Chen, Z., Milner, T.E., Dave, D., and Nelson, J.S. (1997) "Optical Doppler Tomographic Imaging of Fluid Flow Velocity in Highly Scattering Media," *Opt. Lett.* 22, pp. 64–66.

Chien, R. (2003) "Sample Stacking Revisited: A Personal Perspective," *Electrophoresis* 24, pp. 486–97.

Cho, S.K. and Kim, C.-J. (2003), "Particle Separation and Concentration Control for Digital Microfluidic Systems," *Proc Sixteenth Ann. Conf. on MEMS, MEMS-03*, 19–23 January, Kyoto, Japan, pp. 686–89.

Choi, C.-H., Westin, K.J.A., and Breuer, K.S. (2003) "Apparent Slip Flows in Hydrophilic and Hydrophobic Microchannels," *Phys. Fluids* 15, pp. 2897–2902.

Choi, S.B., Barron, R.F., and Warrington, R.O. (1991) "Fluid Flow and Heat Transfer in Microtubes," in DSC-Vol. 32, Micromechanical Sensors, Actuators and Systems, ASME Winter Annual Meeting, Atlanta, Georgia, pp. 123–34.

Chou, C.-F., Austin, R.H., Bakajin, O., Tegenfeldt, J.O., Castelino, J.A., Chan, S.S., Cox, E.C., Craighead, H., Darnton, N., Duke, T., Han, J., and Turner, S. (2000) "Sorting Biomolecules with Microdevices," *Electrophoresis* 21, pp. 81–90.

Cui, H.-H., Silber-Li, Z.-H., and Zhu, S.-N. (2004) "Flow Characteristics of Liquids in Microtubes Driven by a High Pressure," *Phys. Fluids* 16, pp. 1803–10.

Cummings, E.B. and Singh, A.K. (2003) "Dielectrophoresis in Microchips Containing Arrays of Insulating Posts: Theoretical and Experimental Results," *Anal. Chem.* 75, pp. 4724–31.

Cummings, E.B., Griffiths, S.K., and Nilson, R.H. (1999) "Irrotationality of Uniform Electroosmosis," in *SPIE Conference on Microfluidic Devices and Systems II*, Santa Clara, California, 3877, pp. 180–89. AQ22

Cummings, E.B., Griffiths, S.K., Nilson, R.H., et al. (2000) "Conditions for Similitude Between the Fluid Velocity and Electric Field in Electroosmotic Flow," *Anal. Chem.* 72, pp. 2526–32.

Darbyshire, A.G. and Mullin, T. (1995) "Transition to Turbulence in Constant-Mass-Flux Pipe Flow," *J. Fluid Mech.* 289, pp. 83–114.

Devasenathipathy, S., and Santiago, J.G. (2000) unpublished results, Stanford University, Stanford, California, October.

Devasenathipathy, S., Santiago, J.G., and Takehara, K. (2002) "Particle Tracking Techniques for Electrokinetic Microchannel Flows," *Anal. Chem* 74, pp. 3704–13.

Devasenathipathy, S., Santiago, J.G., Wereley, S.T., Meinhart, C. D., and Takehara, K. (2003) "Particle Imaging Techniques for Microfabricated Fluidic Systems," *Exp. Fluids* 34, pp. 504–14.

Dutta, P., Beskok, A., and Warburton, T.C. (2002) "Electroosmotic Flow Control in Complex Microgeometries," *J. Microelectromechanical Systems* 11, pp. 36–44.

Ermakov, S.V., Jacobson, S.C. and Ramsey, J.M. (2000) "Computer Simulations of Electrokinetic Injection Techniques in Microfluidic Devices," *Anal. Chem.* 72, pp. 3512–17.

Everaerts, F.M., Beckers, J.L., and Verheggen, T.P.E.M. (1976) *Isotachophoresis: Theory, Instrumentation, and Applications*, Amsterdam, New York.

Fiechtner, G.J. and Cummings, E.B. (2003) "Faceted Design of Channels for Low-Dispersion Electrokinetic Flows in Microfluidics Systems," *Anal. Chem.* 75, 4747–55.

Flockhart, S.M. and Dhariwal, R.S. (1998) "Experimental and Numerical Investigation into the Flow Characteristics of Channels Etched in <100> Silicon," *J. Fluids Eng.* 120, pp. 291–95.

Fu, L.-M., Yang, R.-J., Lin, C.-H., Pan, Y.-J., and Lee, G.-B. (2004) "Electrokinetically Driven Micro Flow Cytometers with Integrated Fiber Optics for On-Line Cell/Particle Detection," *Anal. Chimica Acta* 507, pp. 163–69.

Gad-el-Hak, M. (1999) "The Fluid Mechanics of Microdevices: The Freeman Scholar Lecture," *J. Fluids. Eng.* 121, pp. 5–33.

Galambos, P. and Forster, F.K. (1998) "Micro-Fluidic Diffusion Coefficient Measurement," in *Micro Total Analysis Systems*, eds. D.J. Harrison and A. van den Berg, Kluwer Academic Publishers, Dordrecht, pp. 189–192.

Gan, W., Yang, L., He, Y., Zeng, R., Cervera, M.L., and d. l. Guardia, M. (2000) *Talanta* 51, p. 667.

Ghosal, S. (2002) "Lubrication Theory for Electro-Osmotic Flow in a Microfluidic Channel of Slowly Varying Cross-Section and Wall Charge," *J. Fluid Mech.* 459, pp. 103–28.

Ghosal, S. (2004) "Fluid Mechanics of Electroosmotic Flow and its Effects on Band Broadening in Capillary Electrophoresis," *Electrophoresis* 25, pp. 214–28.

Glückstad, J. (2004) "Sorting Particles with Light," *Nature Materials* 3, pp. 9–10.

Gray, B., Jaeggi, D., Mourlas, N., van Drieenhuizen, B., Williams, K., Maluf, N., and Kovacs, G.S. (1999) [AQ23] *Sensors and Actuators A- Physical* 77, pp. 57–65.

Green, N.G., Ramos, A., Gonzales, A., Castellanos, A. and Morgan, H. (2000a) "Electric-Field-Induced Fluid Flow on Microelectrodes: The Effects of Illumination," *Journal Phys. D: Applied Physics* 33, pp. L13–17.

Green, N.G., Ramos, A., Gonzales, A., Morgan, H., and Castellanos, A. (2000b) "Fluid Flow Induced by Non-Uniform AC Electric Fields in Electrolytes on Microelectrodes: Part 1, Experimental Measurements," *Phys. Rev. E* 61, pp. 4011–18.

Griffiths, S.K. and Nilson, R.H. (2001) "Low Dispersion Turns and Junctions for Microchannel Systems," *Anal. Chem.* 73, pp. 272–78.

Grushka, E., McCormick, R.M., and Kirkland, J.J. (1989) "Effect of Temperature Gradients on the Efficiency of Capillary Zone Electrophoresis Separations," *Anal. Chem.* 61, pp. 241–46.

Hagen, G. (1839) *On the Motion of Water in Narrow Cylindrical Tubes*, (German) *Pogg. Ann.* 46, p. 423.

Hanks, R.W. and Ruo, H.-C. (1966) "Laminar-Turbulent Transition in Ducts of Rectangular Cross Section," *I&EC Fundamentals* 5, p. 558–61.

Harley, J.C., Huang, Y., Bau, H.H., and Zemel, J.N. (1995) "Gas Flow in Micro-channels," *J. Fluid Mech.* 284, pp. 257–74.

Hayes, M., Kheterpal, I., and Ewing, A. (1993) "Effects of Buffer pH on Electoosmotic Flow Control by an Applied Radial Voltage for Capillary Zone Electrophoresis," *Anal. Chem.* 65, pp. 27–31.

Henry, D.C. (1948) "The Electrophoresis of Suspended Particles: 4, The Surface Conductivity Effect," *Trans. Faraday Soc.* 44, pp. 1021–26.

Herr, A.E., Molho, J.I., Drouvalakis, K.A., Mikkelsen, J.C.,Utz, P.J., Santiago, J.G., and Kenny, T.W. (2003) "On-Chip Coupling of Isoelectric Focusing and Free Solution Electrophoresis for Multi-Dimensional Separations," *Anal. Chem.* 75, pp. 1180–87.

Herr, A.E., Molho, J.I., Santiago, J.G., et al. (2000) "Electroosmotic Capillary Flow with Nonuniform Zeta Potential," *Anal. Chem.* 72, pp. 1053–57.

Hiemenz, P.C. and Rajagopalan, R. (1997) "Principles of Colloid and Surface Chemistry," 3rd ed., Marcel Dekker, Inc., New York.

Hirokawa, T., Okamoto, H., and Gas, B. (2003) "High-Sensitive Capillary Zone Electrophoresis Analysis Bb Electrokinetic Injection with Transient Isotachophoretic Preconcentration: Electrokinetic Supercharging," *Electrophoresis* 24, pp. 498–504.

Hitt, D.L. and Lowe, M.L. (1999) "Confocal Imaging of Flows in Artificial Venular Bifurcations," *Trans. ASME J. Biomech. Eng.* 121, pp. 170–77.

Ho, C.-M. and Tai, Y.-C. (1998) "Micro-Electro-Mechanical Systems (MEMS) and Fluid Flows," *Annu.* [AQ24] *Rev. Fluid Mech.* 30, pp. 279–612.

Hofmann, O., Che, D.P., Cruickshank, K.A., and Muller, U.R. (1999) "Adaptation of Capillary Isoelectric Focusing Tt Microchannels Oo a Glass Chip," *Anal. Chem.* 71, pp. 678–86.

Hsieh, S.-S., Lin, C.-Y., Huang, C.-F., and Tsai, H.-H. (2004) "Liquid Flow in a Micro-Channel," *J. Micromech. Microeng.* 14, pp. 436–45.

Huang, T., Tsai, P., Wu, Ch., and Lee, C. (1993) "Mechanistic Studies of Electroosmotic Control at the Capillary-Solution Interface," *Anal. Chem.* 65, pp. 2887–93.

Hunter, R.J. (1981) "Zeta Potential in Colloid Science," Academic Press, London.

Israelachvili, J.N. (1986) "Measurement of the Viscosity of Liquids in Very Thin Films," *J. Coll. Interface Sci.* 110, pp. 263–71.

Ivory, C.F. (2000). "A Brief Review of Alternative Electrofocusing Techniques," *Separation Science and Technology* 35, pp. 1777–93.

Jacobson, S.C., Hergenroder, R., Moore, A.W. Jr., and Ramsey, J.M. (1994) "Precolumn Reactions with Electrophoretic Analysis Integrated on a Microchip," *Anal. Chem.* 66, pp. 4127–32.

Janson, S.W., Helvajian, H., and Breuer, K. (1999) "MEMS, Microengineering and Aerospace Systems," in 30th AIAA Fluid Dyn. Conf., 28 June–1 July, Norfolk, Virginia, AIAA 99-3802.

Jiang, X.N., Zhou, Z.Y., Yao, J., Li, Y., and Ye, X.Y. (1995) "Micro-Fluid Flow in Microchannel," in *Transducers '95:Eurosensor IX*, 8th Intl. Conf. on Solid-State Sensors and Actuators, and Eurosensors IX, Sweden, pp. 317–20.

Judy, J., Maynes, D. and Webb, B.W. (2002) "Characterization of Frictional Pressure Drop for Liquid Flows through Microchannels," *Int. J. Heat Mass Trsfr* 45, pp. 3477–89.

Jung, B., Bharadwaj, R. and Santiago, J.G. (2003) "Thousand-Fold Signal Increase Using Field Amplified Sample Tacking for On-Chip Electrophoresis," *Electrophoresis* 24, pp. 3476–83.

Kaniansky, D., Masar, M., Bielcikova, J., Ivanyi, F., Eisenbeiss, F., Stanislawski, B., Grass, B., Neyer, A., and Johnck, M. (2000) "Capillary Electrophoresis Separations on a Planar Chip with the Column-Coupling Configuration Separation Channels," *Anal. Chem.* 72, pp. 3596–3604.

Khaledi, M.G. (1998) "High-Performance Capillary Electrophoresis," in *Chemical Analysis: A Series of Monographs on Analytical Chemistry and its Applications*, ed. J.D. Winefordner, p. 146, John Wiley & Sons, Inc., New York.

Kirby, B.J. (2004) "Zeta Potential of Microfluidic Substrates: 1. Theory, Experimental Techniques, and Effects on Separations," *Electrophoresis* 25, pp. 187–202.

Kitahara, A. and Watanabe, A. (1984) *Electrical Phenomena at Interfaces: Fundamentals, Measurements, and Applications*, Surfactant Science Series 15, Marcel Dekker, New York.

Knox, J.H. (1988) "Thermal Effects and Band Spreading in Capillary Electro-Separation," *Chromatographia* 26, pp. 329–37.

Kohlrausch, F. (1897) *Ann. Phys.* (Leipzig) 62, pp. 209–39.

Koo, J. and Kleinstreuer, C. (2003) "Liquid Flow in Microchannels: Experimental Observations and Computational Analyses of Microfluidics Effects," *J. Micromech. Microeng.* 13, pp. 568–79.

Koutsiaris, A.G., Mathiouslakis, D.S., and Tsangaris, S. (1999) "Microscope PIV for Velocity-Field Measurement of Particle Suspensions Flowing inside Glass Capillaries," *Meas. Sci. & Technol.* 10, pp. 1037–46.

Krulevitch, P., Bennett, W., Hamilton, J., Maghribi, M., and Rose, K. (2002) "Polymer-Based Packaging Platform for Hybrid Microfluidic Systems," *Biomedical Microdevices* 4, pp. 301–8.

Landers, J.P. (1994) *Handbook of Capillary Electrophoresis*, CRC Press, Boca Raton, FL.

Lanzillotto, A.-M., Leu, T.-S., Amabile, M., and Wildes, R. (1996) "An Investigation of Microstructure and Microdynamics of Fluid Flow in MEMS," in AD-Vol. 52, Proc. of ASME Aerospace Division, Atlanta, Georgia, pp. 789–96.

Laser, D. and Santiago, J.G. (2004) "A Review of Micropumps," *J. Micromech. and Microeng.* 14, pp. R35–R64.

Lee, G.-B., Hung, C.-I., Ke, B.-J., Huang, G.-R., Hwei, B.-H. and Lai, H.-F. (2001) "Hydrodynamic Focusing for a Micromachined Flow Cytometer," *J. Fluids Eng.* 123, pp. 672–79.

Lee, G.-B., Lin, C.-H., and Chang, G.-L. (2003) "Micro Flow Cytometers with Buried SU-8/SOG Optical Waveguides," *Sensors and Actuators A* 103, pp. 165–70.

Levich, V. (1962) *Physicochemical Hydrodynamics*, Prentice-Hall.

Li, Y., Buch, J.S., Rosenberger, F., DeVoe, D.L., and Lee, C.S. (2004) "Integration of Isoelectric Focusing with Parallel Sodium Dodecyl Sulfate Gel Electrophoresis for Multidimensional Protein Separations in a Plastic Microfluidic Network," *Anal. Chem.* 76, pp. 742–48.

Li, Z.-X., Du, D.-X., and Guo, Z.-Y. (2003) "Experimental Study on Flow Characteristics of Liquid in Circular Microtubes," *Microscale Thermophys. Eng.* 7, pp. 253–65.

Lichtenberg, J., Verpoorte, E., and de Rooij, N.F. (2001) "Sample Preconcentration by Field Amplification Stacking for Microchip-Based Capillary Electrophoresis," *Electrophoresis* 22, pp. 258–71.

Lin, H., Storey, B., Oddy, M., Chen, C.-H. and Santiago, J.G. (2004) "Instability of Electrokinetic Microchannel Flows with Conductivity Gradients," *Physics of Fluids* 16, pp.1922–35.

Liu, D. and Garimella, S.V. (2004) "Investigation of Liquid Flow in Microchannels," *J. Thermophys. Heat Transfer* 18, pp. 65–72.

Liu, R.H., Stremler, M.A., Sharp, K.V., Olsen, M.G., Santiago, J.G., Adrian, R.J., Aref, H., and Beebe, D.J. (2000) "Passive Mixing in a Three-Dimensional Serpentine Microchannel," *J. MEMS* 9, pp. 190–97.

MacInnes, J., Du, X. and Allen, R. (2003) "Prediction of Electrokinetic and Pressure Flow in a Microchannel T-Junction," *Phys. Fluids* 15, pp. 1992–2005.

Macounova, K., Cabrera, C.R. and Yager, P. (2001) "Concentration and Separation of Proteins in Microfluidic Channels on the Basis of Transverse IEF," *Anal. Chem.* 73, pp. 1627–33.

Mala, G.M. and Li, D. (1999) "Flow Characteristics of Water in Microtubes," *Int. J. Heat and Fluid Flow* 20, pp. 142–48.

Manz, A., Effenhauser, C.S., Burggraf, N., et al. (1994) "Electroosmotic Pumping and Electrophoretic Separations for Miniaturized Chemical Analysis Systems," *J. Micromech. Microeng.* 4, pp. 257–65.

Maynes, D. and Webb, A.R. (2002) "Velocity Profile Characterization in Sub-Millimeter Diameter Tubes Using Molecular Tagging Velocimetry," *Exp. Fluids* 32, pp. 3–15.

Meinhart, C.D., Wereley, S.T., and Santiago, J.G. (1999) "PIV Measurements of a Microchannel Flow," *Exp. Fluids* 27, pp. 414–19.

Melcher, J.R. (1981) *Continuum Electromechanics*. MIT Press, Boston.

Merkle, C.L., Kubota, T. and Ko, D.R.S. (1974) "An Analytical Study of the Effects of Surface Roughness on Boundary-layer Transition," AF Office of Scien. Res. Space and Missile Sys. Org., AD/A004786.

Mikkers, F.E.P., Everaerts, F.M., and Verheggen, T. (1979) "High-Performance Zone Electrophoresis," *J. Chromatography* 169, pp. 11–20.

Mirowski, W., Moreland, J., Russek, S.E. and Donahue, M.J. (2004) "Integrated Microfluidic Isolation Platform for Magnetic Particle Manipulation in Biological Systems," *App. Phys. Lett.* 84, pp. 1786–88.

Mohammadi, B., Molho, J.I. and Santiago, J.G. (2003) "Incomplete Sensitivies for the Design of Minimal Dispersion Fluidic Channels," *Computer Methods in Applied Mechanics and Engineering* 192, pp. 4131–45.

Morgan, H. and Green, N.G. (2003) *AC Electrokinetics: Colloids and Nanoparticles*, Research Studies Press Ltd., Baldock, England.

Morini, G.L. (2004) "Laminar-to-Turbulent Flow Transition in Microchannels," *Microscale Thermophys. Eng.* 8, pp. 15–30.

Myung-Suk, C. and Kwak, H.W. (2003) "Electrokinetic Flow and Electroviscous Effect in a Charged Slit-Like Microfluidic Chan with Nonlinear Poisson-Boltzmann Field," *Korea-Australia Rheology Journal* 15, pp. 83–90.

Nguyen, N.-T. and Wereley, S. (2002) *Fundamentals and Applications of Microfluidics*, Artech House, Norwood, MA.

Novotny, E.J. and Eckert, R.E. (1974) "Rheological Properties of Viscoelastic Fluids from Continuous Flow through a Channel Approximating Infinite Parallel Plates," *Trans. Soc. Rheol.* 18, pp. 1–26.

Obot, N.T. (2002) "Toward a Better Understanding of Friction and Heat/Mass Transfer in Microchannels: A Literature Review," *Microscale Thermophys. Eng.* 6, pp. 155–73.

Oddy, M. and Santiago, J.G. (2004) "Alternating Electric Field Measurements of Particle Zeta-Potentials in a Microchannel," *J. Colloid and Interface Science* 269, pp.192–204.

Oddy, M.H., Santiago, J.G. and Mikkelsen, J.C. (2001) "Electrokinetic Instability Micromixing," *Anal. Chem.* 73, pp. 5822–32.

Osbourn, D.M., Weiss, D.J. and Lunte, C.E. (2000) "On-Line Preconcentration Methods for Capillary Electrophoresis," *Electrophoresis* 21, pp. 2768–79.

Overbeek, J.T.G. (1952) "Electrochemistry of the Double Layer," in *Colloid Science*, ed. H.R. Kruyt, Elsevier, Amsterdam, pp. 115–277.

Ovryn, B. (1999) "Three-Dimensional Forward Scattering Particle Image Velocimetry in a Microscopic Field-of-View," in *Proc. 3rd Intl. Workshop PIV*, 16–18 September, Santa Barbara, California, pp. 385–93.

Papautsky, I., Brazzle, J., Ameel, T., and Frazier, A.B. (1999a) "Laminar Fluid Behavior in Microchannels Using Micropolar Fluid Theory," *Sensors and Actuators* 73, pp. 101–8.

Papautsky, I., Gale, B.K., Mohanty, S., Ameel, T.A., and Frazier, A.B. (1999b) "Effects of Rectangular Microchannel Aspect Ratio on Laminar Friction Constant," in *SPIE Conference on Microfluidic Devices and Systems II*, Santa Clara, California, 3877, pp. 147–58.

Patankar, N.A. and Hu, H.H. (1998) "Numerical Simulation of Electroosmotic Flow," *Anal. Chem.* 70, pp. 1870–81.

Paul, P.H., Arnold, D.W., and Rakestraw, D.J. (1998a) "Electrokinetic Generation of High Pressures Using Porous Microstructures," in *Micro Total Analysis Systems*, ed. D.J. Harrison and A. van den Berg, Kluwer Academic Publishers.

Paul, P.H., Garguilo, M.G., and Rakestraw, D.J. (1998b) "Imaging of Pressure- and Electrokinetically Driven Flows Through Open Capillaries," *Anal. Chem.* 70, pp. 2459–67.

Peng, X.F., Peterson, G.P., and Wang, B.X. (1994) "Frictional Flow Characteristics of Water Flowing through Rectangular Microchannels," *Exp. Heat Transfer* 7, pp. 249–64.

Pfahler, J., Harley, J., Bau, H., and Zemel, J. (1990a) "Liquid Transport in Micron and Submicron Channels," *Sensors and Actuators* A21–A23, pp. 431–34.

Pfahler, J., Harley, J., Bau, H., and Zemel, J.N. (1991) "Gas and Liquid Flow in Small Channels," in DSC-Vol. 32, Micromechanical Sensors, Actuators and Systems, ASME Winter Annual Meeting, Atlanta, Georgia, pp. 49–59.

Pfahler, J., Harley, J., Bau, H.H., and Zemel, J. (1990b) "Liquid and Gas Transport in Small Channels," in DSC-Vol. 19, Microstructures, Sensors and Actuators, ASME Winter Annual Meeting, Dallas, Texas, pp. 149–57.

Pfund, D., Rector, D., Shekarriz, A., Popsecu, A., and Welty, J. (2000) "Pressure Drop Measurements in a Microchannel," *AIChE J* 46, pp. 1496–1507.

Phares, D.J. and Smedley, G.T. (2004) "A Study of Laminar Flow of Polar Liquids through Circular Microtubes," *Phys. Fluids* 16, pp. 1267–72.

Poiseuille, M. (1840, 1841) "Recherches Expérimentales Sur le Mouvement des Liquides dans les Tubes de Très Petits Diametrès," *CR Hebdomaires des Séances Acad. Sci.* 11.

Probstein, R.F. (1994) *Physicochemical Hydrodynamics: An Introduction*, 2nd ed., John Wiley & Sons, Inc., New York.

Qu, W., Mala, G.M., and Li, D. (2000) "Pressure-Driven Water Flows in Trapezoidal Silicon Microchannels," *Int. J. Heat and Mass Transfer* 43, pp. 353–64.

Quirino, J. and Terabe, S. (1999) "Sample Stacking of Fast-Moving Anions in Capillary Zone Electrophoresis with pH-Suppressed Electroosmotic Flow," *J. Chromatography A* 850, pp. 339–44.

Ramos, A., Morgan, H., Green, N.G. and Castellanos, A. (1998) "AC Electrokinetics: A Review of Forces in Microelectrode Structures," *J. Physics D: Applied Physics* 21, pp. 2338–53.

Ramos, A., Morgan, H. Green, N.G., and Castellanos, A. (1999) "AC Electric-Field-Induced Fluid Flow in Microelectrodes," *J. Coll. Int. Sci.* 21, pp.: 420–22.

Ren, L., Qu, E. and Li, D. (2001) "Interfacial Electrokinetic Effects on Liquid Flow in Microchannels," *Int. J. Heat Mass Trsfr* 44, pp. 3125–34.

Reyes, D.R., Iossifidis, D., Auroux, P.A., and Manz, A. (2002) "Micro Total Analysis Systems: 1. Introduction, Theory, and Technology," *Anal. Chem.* 74, pp. 2623–36.

Reynolds, O. (1883) "An Experimental Investigation of the Circumstances which Determine whether the Motion of Water Will Be Direct or Sinuous, and the Law of Resistance in Parallel Channels," *Phil. Trans. Roy. Soc. London* 2, p. 51.

Rice, C.L. and Whitehead, R. (1965) "Electrokinetic Flow in a Narrow Cylindrical Capillary," *J. Phys. Chem.* 69, pp. 4017–24.

AQ28

AQ29

AQ30

Righetti, P.G. (1983) *Isoelectric Focusing: Theory, Methodology, and Applications*, Amsterdam, New York.

Ross, D. and Locascio, L.E. (2004) "Microfluidic Temperature Gradient Focusing," *Anal. Chem.* 74, pp. 2556–65.

Russel, W.B., Saville, D.A., and Schowalter, W.R. (1999) "Colloidal Dispersions," *Cambridge Monographs on Mechanics and Applied Mathematics,* ed. G.K. Batchelor, Cambridge University Press. **AQ31**

Santiago, J.G. (2001) "Electroosmotic Flows in Microchannels with Finite Inertial and Pressure Forces," *Anal. Chem.* 73, pp. 2353–65.

Santiago, J.G., Wereley, S.T., Meinhart, C.D., Beebe, D.J., and Adrian, R.J. (1998) "A Particle Image Velocimetry System for Microfluidics," *Exp. Fluids* 25, pp. 316–19.

Saville, D. (1997) "Electrohydrodynamics: The Taylor-Melcher Leaky Dielectric Model," *Annu. Rev. Fluid Mech.* 29, pp. 27–64.

Scales, P., Grieser, F., and Healy, T. (1992) "Electrokinetics of the Silica-Solution Interface: A Flat Plate Streaming Potential Study," *ACS J. Langmuir Surf. Colloids* 8, pp. 965–74.

Schaller, Th., Bolin, L., Mayer, J., and Schubert, K. (1999) "Microstructure Grooves with a Width Less than 50 m Cut with Ground Hard Metal Micro End Mills," *Precision Engr.* 23, pp. 229–35.

Schulte, T.H., Bardell, R.L., and Weigl, B.H. (2000) "On-Chip Microfluidic Sample Preparation," *J. Laboratory Automation* 5, p. 83. **AQ32**

Shah, R.K., and London, A.L. (1978) "Laminar Flow Forced Convection in Ducts," in series *Adv. in Heat Transfer*, Supp. 1, Academic Press, New York.

Sharp, K.V. and Adrian, R.J. (2004) "Transition from Laminar to Turbulent Flow in Liquid Filled Microtubes," *Exp. Fluids* 36, pp. 741–47.

Smoluchowski, M.V. (1903) Bull. Akad. Sci. Cracovie, Classe Sci. Math. Natur., 1 p. 182.

Sobhan, C.B. and Garimella, S.V. (2001) "A Comparative Analysis of Studies on Heat Transfer and Fluid Flow in Microchannels," *Microscale Thermophys.* Eng. 5, pp. 293–311.

Sounart, T.L. and Baygents, J.C. (2001) "Electrically-Driven Fluid Motion in Channels With Streamwise Gradients of the Electrical Conductivity," *Colloids and Surfaces A: Physicochemical and Engineering Aspects* 195, pp. 59–75.

Stone, H.A., Stroock, A.D. and Ajdari, A. (2004) "Engineering Flows in Small Devices: Microfluidics toward a Lab-on-a-Chip," *Ann. Rev. Fluid Mech.* 36, pp. 381–411.

Tan, W., Fan, Z.H., Qiu, C.X., Ricco, A.J. and Gibbons, I. (2002) "Miniaturized Capillary Isoelectric Focusing in Plastic Microfluidic Devices," *Electrophoresis* 23, pp. 3638–45.

Taylor, J.A. and Yeung, E.S. (1993) "Imaging of Hydrodynamic and Electrokinetic Flow Profiles in Capillaries," *Anal. Chem.* 65, pp. 2928–32.

Theeuwes, F. (1987) *J. Pharmaceutical Science* 64. **AQ33**

Tieu, A.K., Mackenzie, M.R., and Li, E.B. (1995) "Measurements in Microscopic Flow with a Solid-state LDA," *Exp. Fluids* 19, pp. 293–94.

Tretheway, D.C. and Meinhart, C.D. (2002) "Apparent Fluid Slip at Hydrophobic Microchannel Walls," *Phys. Fluids* 14, pp. L9–L12.

Tretheway, D.C. and Meinhart, C.D. (2004) "A Generating Mechanism for Apparent Fluid Slip in Hydrophobic Microchannels," *Phys. Fluids* 14, pp. L9–L12.

Tuckerman, D.B. and Pease, R.F.W. (1981) "High-Performance Heat Sinking for VLSI," *IEEE Electron Device Lett.* EDL-2, pp. 126–29.

Vreeland, W.N., Williams, S.J., Barron, A.E. and Sassi, A.P. (2003) "Tandem Isotachophoresis-Zone Electrophoresis via Base-Mediated Destacking for Increased Detection Sensitivity in Microfluidic Systems," *Anal.Chem.* 75, p. 3059.

Wainright, A., Williams, S.J., Ciambrone, G., Xue, Q.F., Wei, J., and Harris, D. (2002) "Sample Pre-Concentration by Isotachophoresis in Microfluidic Devices," *J. Chromatography A* 979, pp. 69–80.

Wang, D., Sigurdson, M., and Meinhart, C. D. (2004) "Experimental Analysis Of Particle and Fluid Motion in AC Electrokinetics," *Experiments in Fluids*, in press.

Weigl, B.H., and Yager, P. (1999) "Microfluidic Diffusion-Based Separation and Detection," *Science* 283, pp. 346–47.

White, F.M. (1994) *Fluid Mechanics,* 3rd ed., McGraw-Hill, Inc., New York.

White, F.M. (1991) *Viscous Fluid Flow*, 2nd ed., McGraw-Hill Series in Mechanical Engineering, eds. J.P. Holman and J.R. Lloyd, McGraw-Hill, New York.

Wilding, P., Pfahler, J., Bau, H.H., Zemel., J.N., and Kricka, L.J. (1994) "Manipulation and Flow of Biological Fluids in Straight Channels Micromachined in Silicon," *Clin. Chem.* 40, pp. 43–47.

Woei, T., Fan, H.Z, Qiu, C.X., Ricco, A.J. and Gibbons, I. (2002) "Miniaturized Capillary Isoelectric Focusing in Plastic Microfluidic Devices," *Electrophoresis* 23, pp. 3638–45

Wu, P. and Little, W.A. (1983) "Measurement of Friction Factors for the Flow of Gases in Very Fine Channels Used for Microminiature Joule-Thomson Refrigerators," *Cryogenics* 23, pp. 273–77.

Xu, Z.Q., Ando, T., Nishine, T., Arai, A., and Hirokawa, T. (2003) "Electrokinetic Supercharging Preconcentration and Microchip Gel Electrophoretic Separation of Sodium Dodecyl Sulfate-Protein Complexes," *Electrophoresis* 24, pp. 3821–27.

Yang, H. and Chien, R.-L. (2001) "Sample Stacking in Laboratory-on-a-Chip Devices," *J. Chromatography A* 924, pp.155–63.

Yao, S. and Santiago, J.G. (2003a) "Porous Glass Electroosmotic Pumps: Theory," *J. Colloid and Interface Science* 268, pp.133–42.

Yao, S., Hertzog, D.E., Zeng, S., Mikkelsen, J.C., and Santiago, J.G. (2003b) "Porous Glass Electroosmotic Pumps: Design and Experiments," *J. Colloid and Interface Science* 268, pp.143–53.

Yazdanfar, S., Kulkarni, M.D., and Izatt, J.A. (1997) "High Resolution Imaging of In Vivo Cardiac Dynamics Using Color Doppler Optical Coherence Tomography," *Opt. Ex.* 1, pp. 424–31.

Yu, D., Warrington, R., Barron, R., and Ameel, T. (1995) "An Experimental and Theoretical Investigation of Fluid Flow and Heat Transfer in Microtubes," in *Proc. of ASME/JSME Thermal Engineering Joint Conference*, 19–24 March, Maui, Hawaii, p. 523–30.

Zeng, S., Chen, C., and Mikkelsen, J.C., et al. (2000) "Fabrication and Characterization of Electrokinetic Micro Pumps," in *7th Intersoc. Conf. on Thermal and Thermomech. Phenomena in Electronic Systems*, 23–26 May, Las Vegas, Nevada.

Zhao, T.S. and Liao, Q. (2002) "Thermal Effects on Electro-Osmotic Pumping of Liquids in Microchannels," *J. Micromechanics and Microengineering* 12, pp. 962–70.

Zhu, Y. and Granick, S. (2001) "Viscosity of Interfacial Water," *Phys. Rev. Lett.* 87, pp. 096104-1–096104-4.

AQ34
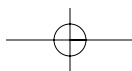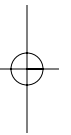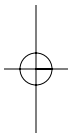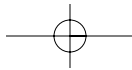
Manuscript Queries

Title: The MEMS Handbook Chapter 10: Liquid Flows in Microchannels		
Page	Query Number	Query
10-4	AQ1	AU: Should Bridgman be included in references?
10-4	AQ2	
10-4	AQ3	AU: Which chapter by Gad-el-Hak?
10-5	AQ4	AU: Brackets OK?
10-7	AQ5	AU: Have I changed your meaning?
10-11	AQ6	AU: Correct as is? Just checking… Also, $\pm$ okay?
10-13	AQ7	AU: 2003, per list of refs.?
10-13	AQ8	AU: mPa rather than MPa? (m = milli-)
10-14	AQ9	AU: please verify equation number.
10-14	AQ10	AU: This chapter title does not appear in TOC.
10-15	AQ11	AU: This chapter title does not appear in TOC.
10-15	AQ12	AU: I can't parse "the lateral resolution was 13.6 μm in the stream-wise direction significantly better 0.9 μm in the cross-stream direction…" Please clarify.
10-16	AQ13	AU: Write out UV and CCD on first appearance?
10-17	AQ14	AU: Please verify equation number.
10-24	AQ15	AU: Smoulochowski or Smoluchowski? It appears both ways; please correct all instances.
10-25	AQ16	AU: Please provide missing character.
10-26	AQ17	AU: Please provide missing character.
10-29	AQ18	AU: Is "400 pl volume" correct as is. Just checking…
10-33	AQ19	AU: Spelling varies throughout your discussion. Please correct all instances.
10-38	AQ20	AU: Is pL correct? See previous query.
10-38	AQ21	AU: please provide editor's name and page nos.
10-39	AQ22	AU: Please provide dates of conference.
10-40	AQ23	AU: Please provide title of article.
10-40	AQ24	AU: Are page nos. correct? Just checking…
10-41	AQ25	AU: Please provide dates of conference and city.
10-41	AQ26	AU: Please provide title of article.

10-41	AQ27	AU: Please provide place of publication.
10-43	AQ28	AU: Please provide dates of conference.
10-43	AQ29	AU: Please provide place of publication.
10-43	AQ30	AU: Should this include page numbers?
10-44	AQ31	AU: Please provide place of publication.
10-44	AQ32	AU: Per text citation; OK?.
10-44	AQ33	AU: Please provide title of article and page nos.
10-45	AQ34	AU: Please provide page nos. if available.
10-2	AQ35	AU: Please provide complete title, facts of publication, etc., as appropriate.
10-3	AQ36	AU: Please provide complete title, facts of publication, etc., as appropriate.
10-12	AQ37	AU: Please provide missing characters.
10-17	AQ38	AU: Please provide complete title, facts of publication, etc., as appropriate.
10-31	AQ39	AU: Should this be bed, per text?